Heteroclinic connections between triple collisions and relative periodic orbits in the isosceles three-body problem

Mitsuru Shibayama† and Kazuyuki Yagasaki‡*

† Research Institute for Mathematical Sciences, Kyoto University, Kyoto 606-8502, Japan

‡ Department of Mechanical and Systems Engineering, Gifu University, Gifu 501-1193, Japan

Abstract. We study the isosceles three-body problem and show that there exist infinitely many families of relative periodic orbits converging to heteroclinic cycles between equilibria on the collision manifold in Devaney's blown-up coordinates. To this end, we prove that two types of heteroclinic orbits exist in much wider parameter ranges than previously detected, using self-validating interval arithmetic calculations, as well as we appeal to the previous results on heteroclinic orbits. Moreover, we give numerical computations for heteroclinic and relative periodic orbits to demonstrate our theoretical results. The numerical results also indicate that the two types of heteroclinic orbits and families of relative periodic orbits exist in wider parameter regions than detected in the theory and that some of them are related to Euler orbits.

E-mail: sibayama@kurims.kyoto-u.ac.jp, yagasaki@ie.niigata-u.ac.jp

July 22, 2009

* Present address: Mathematical Information Division, Department of Information Engineering, Niigata University, Niigata 950-2181, Japan

1. Introduction

We consider the classical three-body problem in the three-dimensional space, for which the equation of motion is given by

$$m_\ell \ddot{\boldsymbol{x}}_\ell = \frac{\partial V}{\partial \boldsymbol{x}_\ell}, \quad \boldsymbol{x}_\ell \in \mathbb{R}^3, \quad \ell = 1, 2, 3, \tag{1.1}$$

where an overdot denotes differentiation with respect to the time variable, m_ℓ (> 0) is the ℓ-th mass and

$$V(\boldsymbol{x}_1, \boldsymbol{x}_2, \boldsymbol{x}_3) = \sum_{i<j} \frac{m_i m_j}{|\boldsymbol{x}_i - \boldsymbol{x}_j|}$$

represents the (negative-)potential energy with the unit gravitational constant. Letting $\boldsymbol{p}_\ell = m_\ell \dot{\boldsymbol{x}}_\ell$ be the momentum of m_ℓ and introducing a state variable vector $\boldsymbol{x} = (\boldsymbol{x}_1, \boldsymbol{x}_2, \boldsymbol{x}_3, \boldsymbol{p}_1, \boldsymbol{p}_2, \boldsymbol{p}_3)$, we write (1.1) as

$$\dot{\boldsymbol{x}} = \boldsymbol{f}(\boldsymbol{x}), \tag{1.2}$$

where

$$\boldsymbol{f}(\boldsymbol{x}) = \left(\frac{1}{m_1}\boldsymbol{p}_1, \frac{1}{m_1}\boldsymbol{p}_2, \frac{1}{m_1}\boldsymbol{p}_3, \frac{\partial V}{\partial \boldsymbol{x}_1}, \frac{\partial V}{\partial \boldsymbol{x}_2}, \frac{\partial V}{\partial \boldsymbol{x}_3} \right).$$

Equation (1.2) (i.e., (1.1)) has several symmetries and permits special classes of solutions called *relative equilibria and relative periodic orbits* as well as true equilibria and periodic orbits.

Let G be a finite-dimensional Lie group such that for any $g \in G$ $\boldsymbol{f}(g\boldsymbol{x}) = g\boldsymbol{f}(\boldsymbol{x})$. For example, we can take a set of all rotations around any axis through the centre of gravity as the Lie group G for (1.2). Obviously, when $\boldsymbol{x}(t)$ is a solution of (1.2), so is $g\boldsymbol{x}(t)$. Let Φ_t denote the flow generated by (1.2). A point $\bar{\boldsymbol{x}}$ is said to lie on a *relative periodic orbit* if there exists $t > 0$ such that $\Phi_t(\bar{\boldsymbol{x}}) \in G\bar{\boldsymbol{x}}$. We say that $T = \inf\{t > 0 \,|\, \Phi_t(\bar{\boldsymbol{x}}) \in G\bar{\boldsymbol{x}}\}$ is the *relative period* of the relative periodic orbit. If $T = 0$, then $\bar{\boldsymbol{x}}$ is said to lie on a *relative equilibrium*. We can regard the set $\{g\Phi_t(\bar{\boldsymbol{x}}), t \in \mathbb{R}, g \in G\}$ as the same relative periodic orbits for all $g \in G$.

Two simplest types of periodic solutions to the three-body problem (1.1) (i.e., (1.2)) were discovered by Euler and Lagrange in the eighteenth century (see chapter 2 of [1]). They are now called Euler and Lagrange orbits after the discoverers' names. In the Euler orbits, three bodies keep a collinear configuration and move homographically like Kepler orbits in an inertial coordinate system. In the Lagrange orbits, the three bodies keep an equilateral triangle configuration. Especially, circular Euler orbits and Lagrange orbits, in which all masses have circular trajectories, are relative equilibria such that the moving bodies rotate rigidly with constant angular velocities around the centre of mass.

As a recent remarkable progress in the three-body problem, Chenciner and Montgomery [2] proved that there exists a figure-eight (periodic) solution. Since then, a number of new periodic and relative periodic orbits in the three-body problem have been obtained. In particular, Chenciner *et. al.* [3] proved the existence of three families

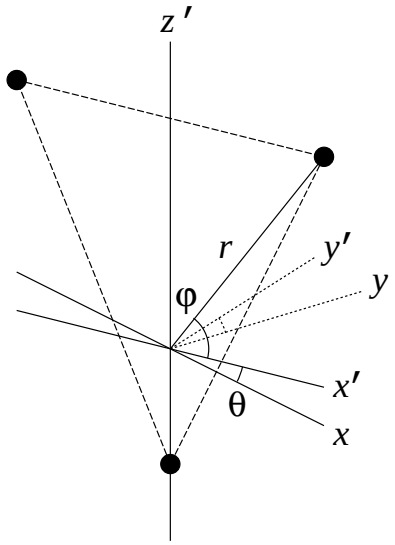

Figure 1. Spatial isosceles three-body problem. The xyz- and $x'y'z$-coordinate systems represent inertial and rotational frames, respectively.

of relative periodic orbits bifurcated from the figure-eight solution while one family was numerically computed by Hénon (see [3]) and the other one (the P_{12} family) was shown theoretically to exist by Marchal [4] earlier. Chenciner and Féjoz [5] also showed that there are Lyapunov families of relative periodic orbits bifurcated from relative equilibria having regular N-gon configurations in the N-body problem with equal masses.

On the other hand, McGehee [6] introduced special coordinates, which are now called *McGehee's coordinates* after him, to blow-up triple collisions and treat them appropriately in the collinear three-body problem. Subsequently, Devaney [7] extended the technique to the so-called *isosceles three-body problem*: two masses are assumed to be equal, $m_1 = m_2$ $(= m)$, and the three bodies maintain an isosceles triangle configuration in which the two equal masses have symmetric positions about an axis passing through the centre of mass (say the z-axis) and the other mass m_3 moves along the axis (see figure 1). Especially, the triple collision singularity was blown-up to an invariant manifold which is called the *collision manifold* and contains some hyperbolic saddle-type equilibria. See section 2.4 for more details. His technique was also used to study orbits near triple collisions in the isosceles three-body problem [7–13]. In particular, the existence of several types of heteroclinic orbits to equilibria on the collision manifold has been proved [9–13] (see also section 3.1). Moeckel [11] also developed a variation on Easton's window theory [14] and proved the existence of an invariant set including relative periodic orbits near heteroclinic cycles. Recently, he remarkably extended the blow-up technique and constructed symbolic dynamics to characterize orbits passing near triple collisions in the planar three-body problem in [15].

In this paper we study the isosceles three-body problem and show that there exist infinitely many families of "symmetric" relative periodic orbits converging to heteroclinic cycles between equilibria on the collision manifold in Devaney's blown-up coordinates. The symmetry of the relative periodic orbits is a new feature, compared with the similar result of Moeckel [11]. To our end, we prove that two types of heteroclinic orbits exist in much wider parameter ranges than detected in [11], using self-validating interval arithmetic calculations [16], as well as we appeal to the previous results of [11, 13] on heteroclinic orbits. Moreover, we give numerical computations for heteroclinic and relative periodic orbits to demonstrate our theoretical results. The numerical results also indicate that the two types of heteroclinic orbits and families of relative periodic orbits exist in wider parameter regions than detected in the theory and that some of them are related to Euler orbits.

The outline of this paper is as follows. In section 2, we review some prerequisites on the isosceles three-body problem: blow-up of the triple collision singularity, reversibility, analytically obtained heteroclinic orbits and the collision manifold. In section 3, we present theoretical results for heteroclinic and relative periodic orbits. We first review the previous results of [11, 13] on the existence of infinitely many heteroclinic orbits to triple collisions and extend another result of Moeckel [11] for other two types of heteroclinic orbits. The technical part based on self-validating interval arithmetic calculations in the proof of the latter is given in appendix A. These heteroclinic orbits are transverse and construct infinitely many heteroclinic cycles. Here we used the terminology "transversality" in a topological meaning and do so through the paper. We next utilize the window theory of Moeckel [11] to show that there exist infinitely many families of relative periodic orbits which converge to the heteroclinic cycles detected. Finally, we give numerical evidence of the theoretical results for heteroclinic and relative periodic orbits in section 4. Our numerical approaches for stable and unstable manifolds, whose intersections yield heteroclinic orbits, and relative periodic orbits are briefly explained. For the computations the computer continuation tool AUTO [18] is effectively used.

2. Isosceles three-body problem

2.1. Equation of motion

In the spatial isosceles three-body problem, we can take the centre of gravity as the origin and the symmetric axis as the z-axis, and assume that the equal masses are located at

$$(x, y, z) \quad \text{and} \quad (-x, -y, z) \tag{2.1}$$

and the other mass m_3 is located at

$$(0, 0, -2\alpha^{-1}z) \tag{2.2}$$

in the inertial coordinate system, where $\alpha = m_3/m$. Note that the constant α is the reciprocal of that used by Moeckel [10, 11].

Letting

$$z' = \sqrt{\frac{\alpha+1}{\alpha}}\, z, \tag{2.3}$$

we introduce the polar coordinate such that

$$x = r\cos\theta\cos\varphi, \quad y = r\sin\theta\cos\varphi, \quad z' = r\sin\varphi \tag{2.4}$$

as in figure 1. We set $m = 1/2$ without a loss of generality and use (1.1) to obtain

$$\begin{aligned} \dot{r} &= vr\cos\varphi, \quad \dot{\varphi} = w, \quad \dot{v} = \left(U(\varphi) - \frac{1}{2}v^2 + 2rh\right)\cos\varphi, \\ \dot{w} &= \frac{\mathrm{d}U}{\mathrm{d}\varphi}(\varphi)\cos^2\varphi - \frac{1}{2}vw\cos\varphi - \left(2U(\varphi) - v^2 + 2rh\right)\sin\varphi\cos\varphi, \end{aligned} \tag{2.5}$$

where h represents the total energy and

$$U(\varphi) = \sec\varphi + \frac{4\alpha^{3/2}}{\sqrt{\alpha + 2\sin^2\varphi}}. \tag{2.6}$$

Here the time variable is changed to eliminate singularities due to mass collisions, and the two variables v and w are related to the velocities in the r- and φ-directions, respectively. Equation (2.5) also has the conservation law

$$\frac{1}{2}\left(v^2\cos^2\varphi + w^2 + \frac{\omega^2}{r}\right) - U(\varphi)\cos^2\varphi = rh\cos^2\varphi, \tag{2.7}$$

where ω represents the angular momentum about the z-axis. Note that the θ-variable does not appear in (2.5) due to its symmetric property.

Devaney [7, 8] introduced the variables (r, φ, v, w) in the planar isosceles three-body problem (i.e. for $\omega = 0$), now called Devaney's coordinates. Subsequently, Moeckel [11] extended them to the spatial isosceles three-body problem (i.e. for $\omega \neq 0$). See [11] for the derivation of (2.5) and (2.7).

2.2. Reversibility and phase space structures

We express (2.5) as

$$\dot{\boldsymbol{\xi}} = \boldsymbol{F}(\boldsymbol{\xi}), \tag{2.8}$$

where $\boldsymbol{\xi} = (r, \varphi, v, w)$. Let

$$R_1 : (r, \varphi, v, w) \mapsto (r, \varphi, -v, -w) \tag{2.9}$$

and let

$$R_2 : (r, \varphi, v, w) \mapsto (r, -\varphi, -v, w). \tag{2.10}$$

They are linear involutions since R_i^2, $i = 1, 2$, are the identity, and they satisfy

$$\boldsymbol{F}(R_i\boldsymbol{\xi}) + R_i\boldsymbol{F}(\boldsymbol{\xi}) = 0, \quad i = 1, 2. \tag{2.11}$$

Thus, the system (2.5) is *reversible* with respect to R_i, $i = 1, 2$ [19]. Let $\mathrm{Fix}(R_i) = \{\boldsymbol{\xi} \in \mathbb{R}^4 \,|\, R_i\boldsymbol{\xi} = \boldsymbol{\xi}\}$ denote the invariant plane for R_i for $i = 1, 2$. We easily see that $\mathrm{Fix}(R_1) = \{v = w = 0\}$ and $\mathrm{Fix}(R_2) = \{\varphi = v = 0\}$.

A fundamental characteristic of reversible systems is that if $\boldsymbol{\xi}(t)$ is a solution, then so is $R_i\boldsymbol{\xi}(-t)$, $i = 1, 2$. We call a solution (and the corresponding orbit) *R_i-symmetric* if $x(t) = R_i\boldsymbol{\xi}(-t)$. Moreover, an orbit is R_i-symmetric if and only if it intersects the space $\mathrm{Fix}(R_i)$ (see [20]).

The function $U(\varphi)$ is even and has three critical points on $(-\pi/2, \pi/2)$, including $\varphi = 0$. Let $\varphi = \pm\varphi_\mathrm{c}$ denote the other critical points of $U(\varphi)$, where

$$\varphi_\mathrm{c} = \arccos\sqrt{\frac{\alpha + 2}{2(2\alpha + 1)}} > 0.$$

The system (2.5) has six equilibria at $C = (0, 0, v_0, 0)$, $C^* = (0, 0, -v_0, 0)$, $E_\pm = (0, \pm\varphi_\mathrm{c}, v_\mathrm{c}, 0)$ and $E_\pm^* = (0, \pm\varphi_\mathrm{c}, -v_\mathrm{c}, 0)$ in the (r, φ, v, w)-phase space, where $v_0 = \sqrt{2U(0)}$ and $v_\mathrm{c} = \sqrt{2U(\varphi_\mathrm{c})}$. We easily see that these equilibria are hyperbolic saddles and satisfy the relations $E_\pm^* = R_1E_\pm$, $E_\pm^* = R_2E_\mp$ and $C = R_iC^*$, $i = 1, 2$. Moreover, $E_\pm$ (resp. $E_\pm^*$) have two-dimensional stable and unstable manifolds, denoted by $W^\mathrm{s}(E_\pm)$ and $W^\mathrm{u}(E_\pm)$ (resp. $W^\mathrm{s}(E_\pm^*)$ and $W^\mathrm{u}(E_\pm^*)$), respectively, while C (resp. C^*) has three-dimensional stable (resp. unstable) manifold denoted by $W^\mathrm{s}(C)$ (resp. $W^\mathrm{u}(C^*)$) and one-dimensional unstable (resp. stable) manifold denoted by $W^\mathrm{u}(C)$ (resp. $W^\mathrm{s}(C^*)$). From the reversibility of (2.5) and the above relations we see that $W^{\mathrm{s,u}}(E_\pm^*) = R_1W^{\mathrm{u,s}}(E_\pm)$, $W^{\mathrm{s,u}}(E_\mp^*) = R_2W^{\mathrm{u,s}}(E_\pm)$ and $W^{\mathrm{s,u}}(C^*) = R_iW^{\mathrm{u,s}}(C)$, $i = 1, 2$.

2.3. Analytically obtained, heteroclinic orbits on invariant planes

Let us assume that $\omega = 0$. We see that the planes $\{\varphi = w = 0\}$ and $\{\varphi = \pm\varphi_\mathrm{c}, w = 0\}$ are invariant for (2.5) since by the energy relation (2.7)

$$\frac{1}{2}v^2 - U_0 = rh, \quad U_0 = U(0) = 4\alpha + 1 \tag{2.12}$$

and

$$\frac{1}{2}v^2 - U_\mathrm{c} = rh, \quad U_\mathrm{c} = U(\varphi_\mathrm{c}) = \sqrt{\frac{2(2\alpha + 1)^3}{\alpha + 2}}, \tag{2.13}$$

so that $\dot\varphi = \dot w = 0$ there. Hence, the system (2.5) reduces to

$$\dot r = vr, \quad \dot v = U_0 - \frac{1}{2}v^2 + 2rh \tag{2.14}$$

on $\{\varphi = w = 0\}$ and

$$\dot r = vr\cos\varphi, \quad \dot v = \left(U_\mathrm{c} - \frac{1}{2}v^2 + 2rh\right)\cos\varphi_\mathrm{c}, \tag{2.15}$$

on $\{\varphi = \pm\varphi_\mathrm{c}, w = 0\}$. Using (2.12) and (2.13), we can rewrite the second equations of (2.14) and (2.15) as

$$\dot v = \frac{1}{2}(v^2 - v_0^2) \tag{2.16}$$

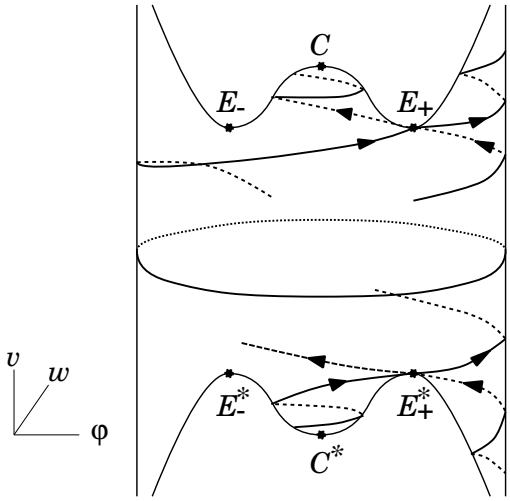

Figure 2. Collision manifold $\mathscr{N}$. Here C, C^*, $E_\pm$ and $E_\pm^*$ represent equilibria in (2.5).

and

$$\dot{v} = \frac{1}{2}\cos\varphi_{\rm c}(v^2 - v_{\rm c}^2), \tag{2.17}$$

which have solutions

$$v = -v_0 \tanh\left(\tfrac{1}{2}v_0\, t\right) \tag{2.18}$$

and

$$v = -v_{\rm c}\tanh\beta t, \quad \beta = \tfrac{1}{2}v_{\rm c}\cos\varphi_{\rm c}, \tag{2.19}$$

respectively. It follows from (2.12) and (2.13) that equations (2.14) and (2.15) have solutions

$$(r, v) = \left(-\frac{v_0^2}{2h}\mathrm{sech}^2(\tfrac{1}{2}v_0\, t), -v_0^2\tanh\left(\tfrac{1}{2}v_0\, t\right)\right) \tag{2.20}$$

and

$$(r, v) = \left(-\frac{v_{\rm c}^2}{2h}\mathrm{sech}^2\beta t, -v_{\rm c}\tanh\beta t\right), \tag{2.21}$$

which give heteroclinic orbits from C to C^* on $\{\varphi = w = 0\}$, and from $E_\pm$ to $E_\pm^*$ on $\{\varphi = \pm\varphi_{\rm c}, w = 0\}$, respectively. These heteroclinic orbits were given earlier in [11] with no explanation.

2.4. Collision manifold

We now give a key concept of a collision manifold in our study. Let

$$\mathscr{E}(\omega) = \tfrac{1}{2}\left(v^2\cos^2\varphi + w^2 + \frac{\omega^2}{r}\right) - U(\varphi)\cos^2\varphi - rh\cos^2\varphi, \tag{2.22}$$

Equation (2.7) defines a three-dimensional manifold

$$\mathscr{M}(\omega) = \{(r, \varphi, v, w) \mid \mathscr{E}(\omega) = 0\},$$

which consists of orbits with angular momentum ω and energy h. Let

$$\mathscr{E}_0 = \tfrac{1}{2}\left(v^2 \cos^2\varphi + w^2\right) - U(\varphi)\cos^2\varphi \tag{2.23}$$

and define

$$\begin{aligned}
\mathscr{M}_+ &= \{(r, \varphi, v, w) \mid r \geq 0, \mathscr{E}(0) = 0\},\\
\mathscr{M}_0 &= \{(r, \varphi, v, w) \mid r = 0, \mathscr{E}_0 > 0\},\\
\mathscr{N} &= \mathscr{M}_+ \cap \mathscr{M}_0 = \{(r, \varphi, v, w) \mid r = 0, \mathscr{E}_0 = 0\},\\
\mathscr{M} &= \mathscr{M}_+ \cup \mathscr{M}_0.
\end{aligned}$$

In particular, we refer to $\mathscr{N}$, which is sketched in figure 2, as a *collision manifold*. The collision manifold was first introduced by Devaney [7, 8], and the other invariant sets by Moeckel [11] later. We regard $\mathscr{M}$ as the limiting variety of $\mathscr{M}(\omega)$ when $\omega \to 0$. Topologically, $\mathscr{N} = \partial\mathscr{M}_0 \cong S^2\backslash\{\text{four points}\}$ and $\mathscr{M}_0 \cong D^3\backslash\{\text{four points}\}$ (which, respectively, represent the surface and the inside domain in figure 2). It is clear that $\mathscr{M}_+$, $\mathscr{M}_0$ and $\mathscr{M}$ are invariant under the flow of (2.5). Moreover, for solutions of (2.5) with $r = 0$ we have

$$\dot{\mathscr{E}}_0 = -\mathscr{E}_0\, v \cos\varphi,$$

from which it follows that $\mathscr{N}$ is also invariant.

All the equilibria given in section 2.2 lie on $\mathscr{N}$. In addition, $W^{\mathrm{s}}(E_\pm), W^{\mathrm{u}}(E_\pm^*) \subset \mathscr{M}_0$ and $W^{\mathrm{u}}(E_\pm), W^{\mathrm{s}}(E_\pm^*) \subset \mathscr{M}_+$, while $W^{\mathrm{s}}(C), W^{\mathrm{u}}(C^*) \subset \mathscr{M}_0$ and $W^{\mathrm{u}}(C), W^{\mathrm{s}}(C^*) \subset \mathscr{M}_+$. See figure 2. Especially, all heteroclinic orbits given in section 2.3 are included in $\mathscr{M}_+$. See [11] for more details.

3. Theoretical results

3.1. Heteroclinic orbits from $E_\pm$ to $E_\pm^*$ or to $E_\mp^*$

We now state theoretical results for the existence of heteroclinic orbits and relative periodic orbits. We begin with heteroclinic orbits.

Moeckel [11] and Shibayama [13] showed that two classes of infinitely many heteroclinic orbits from $E_\pm$ to $E_\pm^*$ or to $E_\mp^*$ exist other than ones in section 2.3. Their results are stated as follows.

Theorem 1 (Moeckel)**.** *For $0 < \alpha < \frac{55}{4}$ there exist infinitely many, R_1- and R_2-symmetric, transverse heteroclinic orbits from $E_\pm$ to $E_\pm^*$ and $E_\pm^*$ passing any neighbourhood of the heteroclinic orbit (2.20) from C to C^*.*

Theorem 2 (Shibayama)**.** *For any $\alpha > 0$ and $k \in \mathbb{N}$, there exists an R_1-symmetric, transverse heteroclinic orbit from $E_\pm$ to $E_\pm^*$ that experiences k binary collisions (i.e., passes $\varphi = \pm\frac{1}{2}\pi$ k times).*

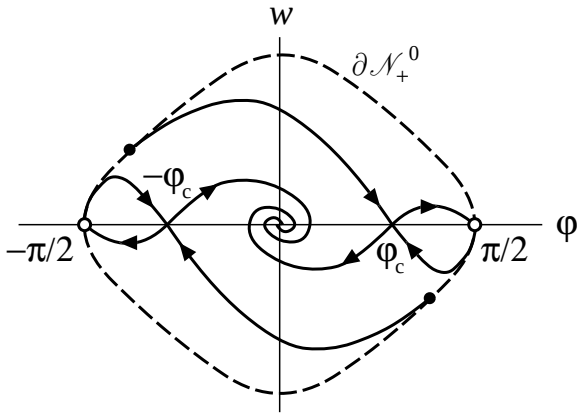

Figure 3. Stable and unstable manifolds of $\bar{E}_\pm$ in (3.1). A situation in the case of $\alpha < \frac{55}{4}$ is depicted: The right branch of $W^{\rm s}(\bar{E}_+)$ end at $(\varphi, w) = (\frac{1}{2}\pi, 0)$ and its left branch touch the above arc of $\partial\mathscr{N}_+$ while the left branch of $W^{\rm s}(\bar{E}_-)$ end at $(-\frac{1}{2}\pi, 0)$ and its right branch touch the lower arc of $\partial\mathscr{N}_+$.

We say that an orbit is *parabolic* if $r \to \infty$, $v \to 0$ and $\varphi \to \pm\frac{\pi}{2}$ as $t \to +\infty$. McGehee [21] showed that the set of all parabolic orbits consists of two two-dimensional analytic manifolds $\mathscr{P}_\pm$ which we now call *parabolic manifolds*. Simó and Martínez [12] also studied the dynamics of (2.5) near $\mathscr{P}_\pm$ and proved the existence of infinitely many heteroclinic orbits around $\mathscr{P}_\pm$. From the proof of [13] it turns out that the heteroclinic orbits obtained in theorem 2 converge to $\mathscr{P}_\pm$ as $k \to \pm\infty$. Thus, for sufficiently large k the heteroclinic orbits in theorem 2 yield the result in [12] although the proof is quite different from theirs.

3.2. Heteroclinic orbits from $E_\pm^*$ to $E_\pm$ and to $E_\mp$

Moeckel [11] proved the existence of heteroclinic orbits from $E_\pm^*$ to $E_\pm$ exist for $\alpha \geq \frac{55}{4}$ and from $E_\pm^*$ to $E_\mp$ for α sufficiently small. We extend his result in the following. We mainly consider the upper region $v \geq 0$ below. The lower region $v \leq 0$ can be analyzed similarly.

We first take the section $\Sigma = \{(r, \varphi, v, w) \mid v = 0\}$, which is convenient to consider since $\mathrm{Fix}(R_1)$ and $\mathrm{Fix}(R_2)$ are contained in it and simply represented as the planes $\{w = 0\}$ and $\{\varphi = 0\}$, respectively, on it. Let $\mathscr{N}_+ = \{(r, \varphi, v, w) \in \mathscr{N} \mid v > 0, -\frac{1}{2}\pi < \varphi < \frac{1}{2}\pi\} \subset \mathscr{N}$. The boundary of $\mathscr{N}_+$ in $\mathscr{N}$ is represented by $\partial\mathscr{N}_+ = \{2U(\varphi)\cos^2\varphi - w^2 = 0\}$ and included by Σ except two points $(\varphi, w) = (\pm\frac{1}{2}\pi, 0)$. The restriction of (2.5) onto $\mathscr{N}_+$ is governed by a two-dimensional system

$$\dot{\varphi} = w, \quad \dot{w} = \frac{dU}{\mathrm{d}\varphi}(\varphi)\cos^2\varphi - \frac{1}{2}w\sqrt{2U(\varphi)\cos^2\varphi - w^2} - w^2\tan\varphi. \tag{3.1}$$

Equation (3.1) has three equilibria at $(\varphi, w) = (0, 0)$ and $(\pm\varphi_{\rm c}, 0)$, which correspond to C and $E_\pm$ and are denoted by $\bar{C}$ and $\bar{E}_\pm$, respectively, and they are all hyperbolic: $\bar{C}$ is a

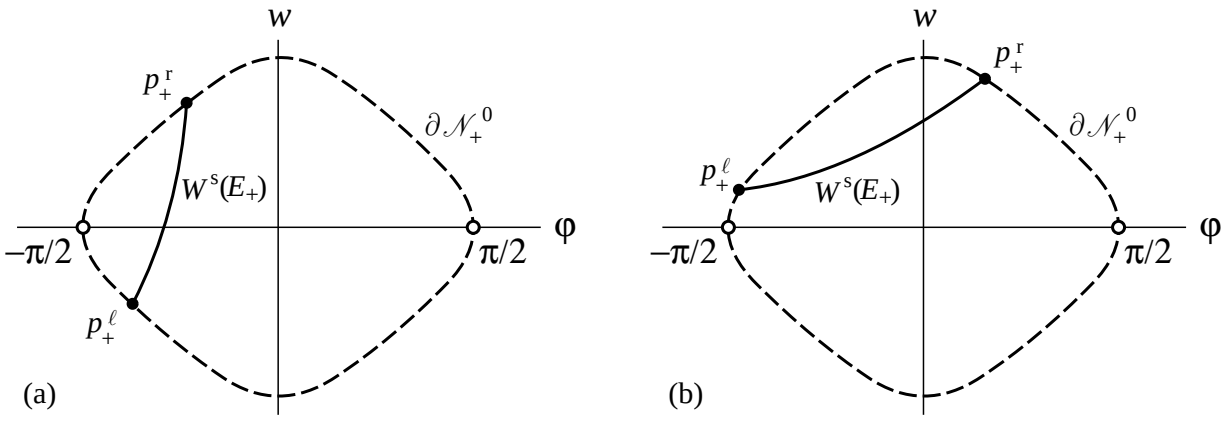

Figure 4. Intersection between $W^{\rm s}(E_\pm)$ and Σ: (a) $\alpha > \alpha_1$; (b) $\alpha < \alpha_2$.

sink which is spiral for $\alpha < \frac{55}{4}$ and non-spiral for $\alpha \geq \frac{55}{4}$, and $\bar{E}_\pm$ are saddles. Moreover, the vector field of (3.1) is tangent to the boundary.

The behaviour of the stable and unstable manifolds of $\bar{E}_\pm$ is drawn in figure 3. The basin of $\bar{C}$ includes the right (resp. left) branch of $W^{\rm u}(\bar{E}_+)$ (resp. $W^{\rm u}(\bar{E}_-)$). The right branches of $W^{\rm s}(\bar{E}_\pm)$ touch the lower arc of $\partial\mathscr{N}_+^0 = \partial\mathscr{N}_+ \backslash \{(\varphi, w) = (\pm\frac{1}{2}\pi, 0)\}$ or end at $(\varphi, w) = (\frac{1}{2}\pi, 0)$ and the left branches of $W^{\rm s}(\bar{E}_\pm)$ touch the upper arc of $\partial\mathscr{N}_+^0$ or end at $(-\frac{1}{2}\pi, 0)$, while the right (resp. left) branch of $W^{\rm u}(\bar{E}_+)$ (resp. $W^{\rm u}(\bar{E}_-)$) must end at $(\frac{1}{2}\pi, 0)$ (resp. at $(-\frac{1}{2}\pi, 0)$) since $\dot{v} > 0$ except at the equilibria and $\varphi = \pm\frac{1}{2}\pi$. See [7,8,11] for the details. Note that there exists no closed orbit encircling the one sink and two saddles by the index theory [22], and that the vector field of (3.1) is antisymmetric about the origin.

Orbits on $W^{\rm s}(\bar{E}_\pm)$ finally intersect the section Σ even if the branches of $W^{\rm s}(\bar{E}_\pm)$ end at $(\varphi, w) = (\pm\frac{1}{2}\pi, 0)$. Let $p_\pm^\ell$ and $p_\pm^{\rm r}$, respectively, denote points on $\partial\mathscr{N}_+$ at which orbits on the left and right branches of $W^{\rm s}(\bar{E}_\pm)$ intersect Σ. Note that $p_\pm^{\ell,{\rm r}}$ may be $(\varphi, w) = (\pm\frac{1}{2}\pi, 0)$. We have the following lemma.

Lemma 1. (i) *There exists a constant $\bar{\alpha}_1 < 6.52$ such that for $\alpha > \bar{\alpha}_1$ p_+^ℓ and $p_+^{\rm r}$, respectively, lie on the lower and upper arcs of $\partial\mathscr{N}_+^0$.*

(ii) *There exists a constant $\bar{\alpha}_2 > 2.25$ such that for $\alpha < \bar{\alpha}_2$ p_+^ℓ and $p_+^{\rm r}$, respectively, lie in the left and right half planes $\{\varphi < 0\}$ and $\{\varphi > 0\}$.*

The proof of this lemma is given in Appendix A. Moeckel [10] also proved the statement of part (i) for $\alpha \geq \frac{55}{4}$.

Since

$$\dot{v} = (-\mathscr{E}_0 + \tfrac{1}{2}w^2)\sec\varphi > 0$$

for $\mathscr{E}_0 < 0$ and $r = 0$, all orbits on $W^{\rm s}(E_\pm) \subset \mathscr{M}_0$ with $\mathscr{E}_0 < 0$ and $v > 0$ must also intersect the section Σ in a point whose projection onto the (φ, w)-space is inside that of

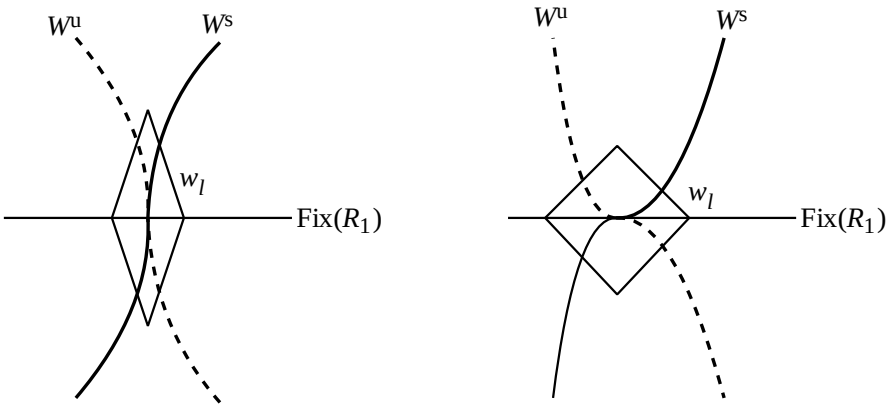

Figure 5. Windows around topologically transverse heteroclinic orbits on Σ.

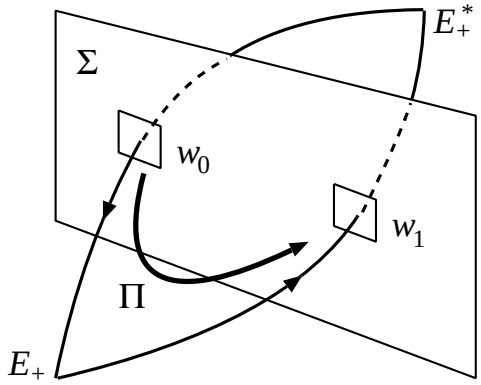

Figure 6. Half return map Π.

$\partial\mathcal{N}_+$. This means that $W^{\mathrm{s}}(E_\pm)$ intersect Σ in a curve whose projection onto the (φ, w)-plane is a curve connecting $p_\pm^{\mathrm{r}}$ and $p_\pm^{\ell}$. Hence, for $\bar{\alpha}_1$ (resp. $\bar{\alpha}_2$) $W^{\mathrm{s}}(E_\pm)$ also intersect the invariant plane Fix(R_1) (resp. Fix(R_2), so that there exists a heteroclinic orbit from $E_\pm^*$ to $E_\pm$ (resp. to $E_\mp$). See figure 4. This proves the following result.

Theorem 3. *There exist two constants $\alpha_1 \le \bar{\alpha}_1$ and $\alpha_2 \ge \bar{\alpha}_2$ such that for $\alpha > \alpha_1$ and $\alpha < \alpha_2$, respectively, there exist R_1- and R_2-symmetric transverse heteroclinic orbits from $E_\pm^*$ to $E_\pm$ and to $E_\mp$, respectively.*

Moeckel proved a similar result for $\alpha_1 < \frac{55}{4} = 13.75$ and $\alpha_2 > 0$ in proposition 3.2 of [11]. Compared with his results, the estimates of theorem 3 on α-intervals for the existence of heteroclinic orbits are very sharp. Simó [9] also showed numerically that the intervals $[\alpha_1, \infty)$ and $[0, \alpha_2]$ overlap in an interval including $\alpha = 1$. In section 4 we will see that our numerical results suggest $\alpha_1 = 0$ and $\alpha_2 = 2.6\ldots$.

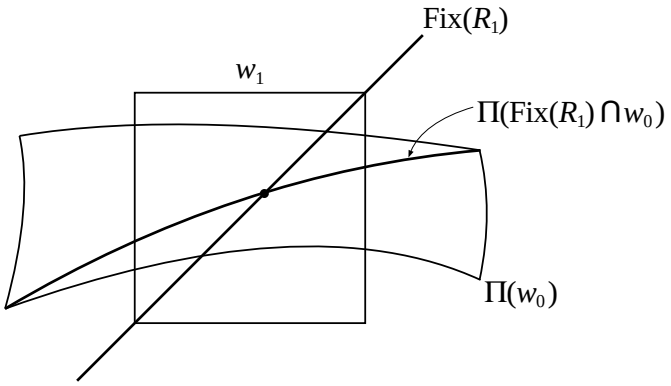

Figure 7. Correctly aligned windows and a symmetric periodic orbit.

3.3. Existence of one-parameter families of periodic orbits

Combining theorems 1 and 2 with theorem 3, we see that there exist infinitely many, R_1-symmetric (resp. R_2-symmetric), transverse heteroclinic cycles connecting $E_\pm$ with $E^*_\pm$ (resp. with $E^*_\mp$) for $\alpha > \alpha_1$ (resp. for $\alpha < \alpha_2$), where $\alpha_1 \leq 6.52$ (resp. $\alpha_2 \geq 2.25$) is given in theorem 3. Using the *window theory* of Moeckel [11], we can prove the existence of infinitely many families of R_1- and R_2-symmetric periodic orbits converging to the R_1- and R_2-symmetric transverse heteroclinic cycles, respectively, when the angular momentum $\omega > 0$ is small, as follows.

Specifically, we consider an R_1-symmetric transverse heteroclinic cycle. A similar argument applies to an R_2-symmetric transverse heteroclinic cycle. First, we choose two small rectangles called *windows*, w_0 and w_1, on Σ near the heteroclinic orbits from E^*_+ to E_+ and from E_+ to E^*_+ for $\omega > 0$, such that a pair of opposite sides of w_0 and w_1 do not intersect $W^{\rm s}(E_+)$ and $W^{\rm u}(E_+)$ (i.e., w_0 and w_1 are plus- and minus-transverse to $W^{\rm s}(E_+)$ and $W^{\rm u}(E_+)$ in his terminologies), respectively, as shown in figure 5. When ω is sufficiently small, the flow of (2.5) intersects w_0 and w_1 transversely in a geometrical meaning since the heteroclinic orbits do. Let Π be the half return map taking a point on w_0 to a point on Σ for the flow of (2.5) (see figure 6). As in [11], we can show that for ω sufficiently small, w_1 and $\Pi(w_0)$ intersect transversely in a topological meaning (i.e., w_0 and w_1 are "correctly aligned" in his terminology). See figure 7. In particular, the image of the diagonal of w_0 intersects that of w_1. Hence, if we choose w_0, w_1 on Σ such that their diagonals are on Fix(R_1), then the intersection point gives a symmetric periodic orbit. Thus, we prove the following.

Theorem 4. *There exist infinitely many families of R_1-symmetric (resp. R_2-symmetric) periodic orbits converging to R_1-symmetric (resp. R_2-symmetric), transverse heteroclinic cycles connecting $E_\pm$ with $E^*_\pm$ (resp. with $E^*_\mp$) given in theorems 1-3 for $\alpha > \alpha_1$ (resp. for $\alpha < \alpha_2$).*

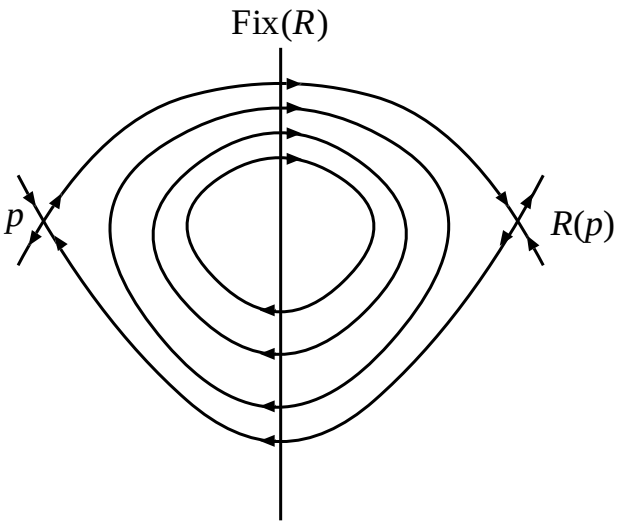

Figure 8. Symmetric transverse heteroclinic cycle and a one-parameter family of symmetric periodic orbits. Here R represents the associated involution, and p and $R(p)$ are a symmetric pair of equilibria.

The situation of theorem 4 is depicted in figure 8. For geometrically transverse heteroclinic cycles, the statement immediately follows from a corollary to theorem A in Devaney [17] by noting that $E^*_\pm = R_1(E_\pm)$ and $E^*_\mp = R_2(E_\pm)$. This theorem also gives infinitely many "new" families of relative periodic orbits which are symmetric about the z-axis (resp. about the z-axis and xy-plane) in the three-dimensional three-body problem (1.1), corresponding to the infinitely many families of R_1-symmetric (resp. R_2-symmetric) periodic orbits in (2.5). Moreover, these families of relative periodic orbits converge to triple collisions.

4. Numerical computations

4.1. Heteroclinic orbits

Now we give numerical evidence of the above theoretical results. We first compute the stable and unstable manifolds and heteroclinic connections.

As stated in section 2.2, if we compute $W^{\mathrm{s,u}}(E_+)$, then we obtain $W^{\mathrm{s,u}}(E^*_+) = R_1 W^{\mathrm{u,s}}(E_+)$, $W^{\mathrm{s,u}}(E^*_-) = R_2 W^{\mathrm{u,s}}(E_+)$ and $W^{\mathrm{s,u}}(E_-) = R_1 W^{\mathrm{u,s}}(E^*_-) = R_1 R_2 W^{\mathrm{s,u}}(E_+)$ by the reversibility. Similarly, we can also apply the involutions $R_{1,2}$ to heteroclinic orbits between E_+ and E^*_+ or E^*_- to get heteroclinic orbits between E_- and E^*_- or E^*_+. So we concentrate only on the computation of $W^{\mathrm{s,u}}(E_+)$ and heteroclinic orbits between E_+ and E^*_+ or E^*_- below.

We begin with $W^{\mathrm{u}}(E_+)$. We first approximate $W^{\mathrm{u}}(E_+)$ by the unstable subspace of

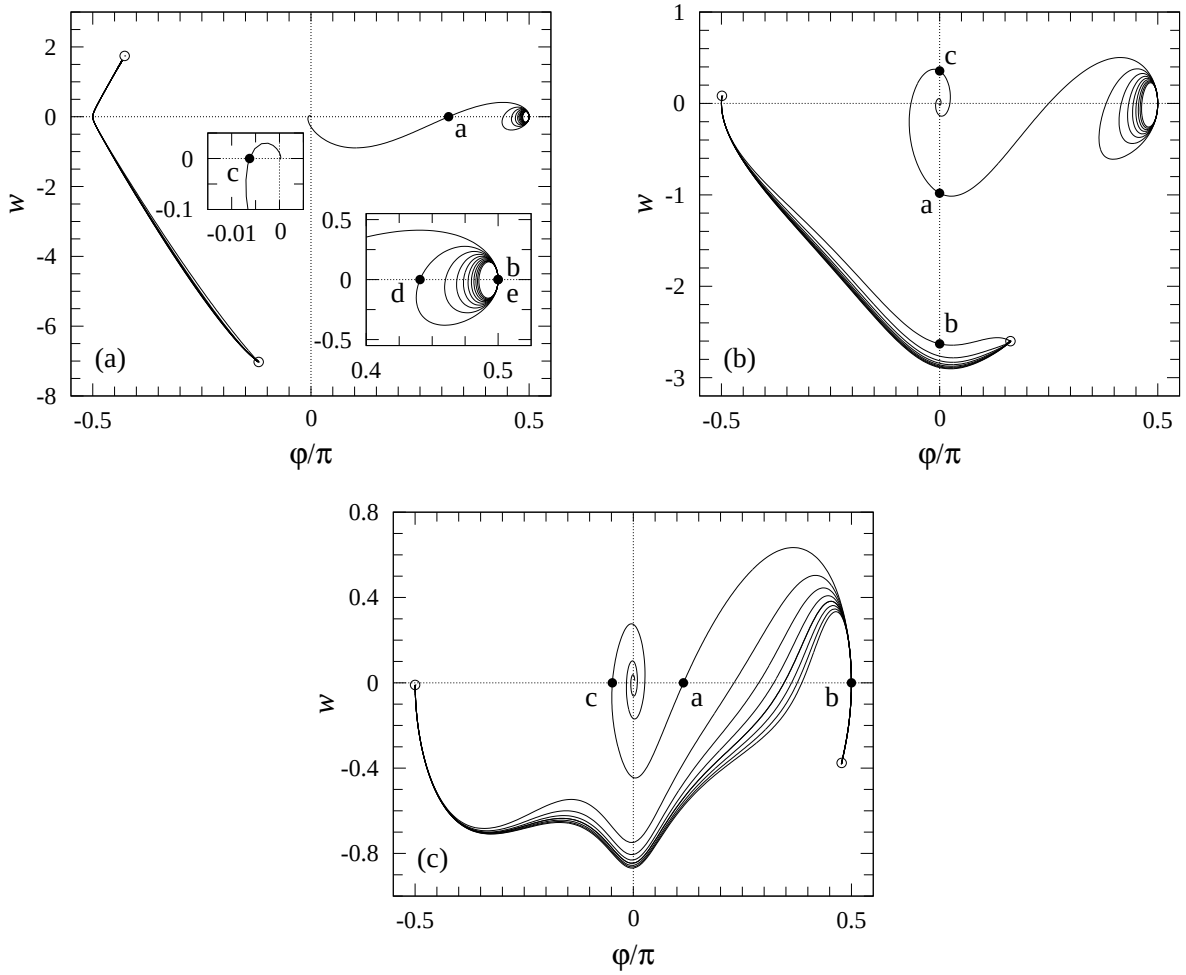

Figure 9. Unstable manifold of E_+ on the section Σ: (a) $\alpha = 7$; (b) $\alpha = 1$; (c) $\alpha = 0.1$. The symbol "$\circ$" represents an orbit with $r = 0$ on $W^{\mathrm{u}}(E_+^*)$, and the symbol "$\bullet$" and alphabetical labels correspond to heteroclinic orbits which are the limits of one-parameter families of periodic orbits in figures 14, 15 and 16.

the linearised system

$$\dot{\boldsymbol{\eta}} = \mathrm{D}\boldsymbol{F}(E_+)\boldsymbol{\eta} \tag{4.1}$$

near $\boldsymbol{\xi} = E_+$. Under this approximation, we obtain an orbit $\boldsymbol{\xi}^{\mathrm{u}}(t)$ on $W^{\mathrm{u}}(E_+)$ as a solution of (2.8) satisfying the boundary condition

$$L_{\mathrm{s}}\boldsymbol{\xi}^{\mathrm{u}}(0) = \boldsymbol{0}, \quad \boldsymbol{\xi}^{\mathrm{u}}(T) = \boldsymbol{\xi}_0^{\mathrm{u}}, \tag{4.2}$$

where $T > 0$ is a constant, L_{s} is an 2×4 matrix consisting of row eigenvectors associated with eigenvalues of negative real parts for the Jacobian matrix $\mathrm{D}\boldsymbol{F}(E_+)$, and $\boldsymbol{\xi}_0^{\mathrm{u}}$ is a point on $W^{\mathrm{u}}(E_+)$. Thus, we solve the boundary value problem (2.8) and (4.2) and continue the solution with $\boldsymbol{\xi}_0^{\mathrm{u}}$ to compute $W^{\mathrm{u}}(E_+)$ numerically. A quite related approach was used to detect 512 heteroclinic connections in the Lorenz model in [23]. This approach can also be extended to compute the unstable manifolds of normally hyperbolic invariant

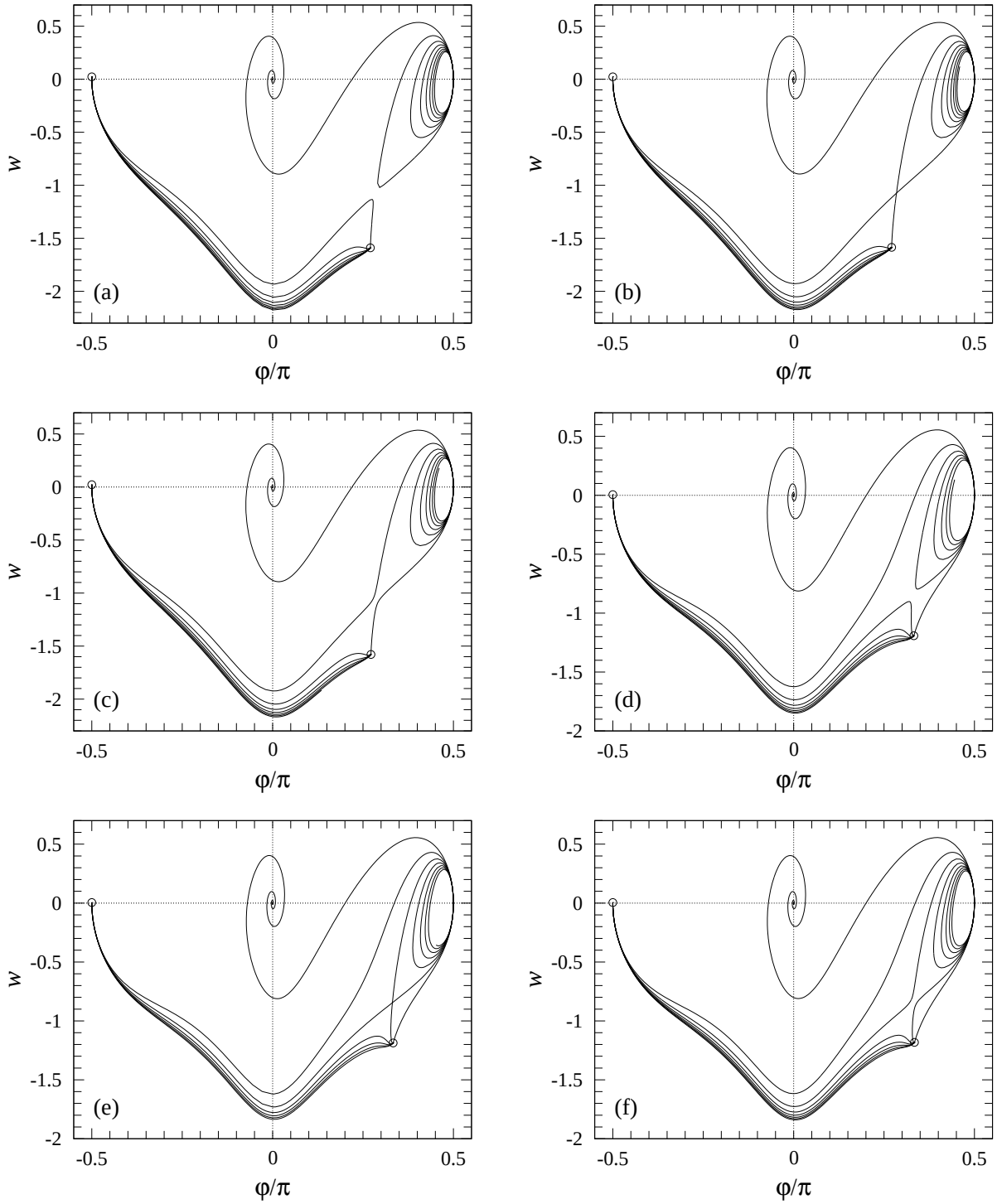

Figure 10. Unstable manifold of E_+ on the section Σ: (a) $\alpha = 0.59$; (b) $\alpha = 0.5884$; (c) $\alpha = 0.586$; (d) $\alpha = 0.434$; (e) $\alpha = 0.43201$; (f) $\alpha = 0.43$. The symbol "$\circ$" represents an orbit with $r = 0$ on $W^{\mathrm{u}}(E_+^*)$.

manifolds [24]. Moreover, if $W^{\mathrm{u}}(E_+)$ intersects $\mathrm{Fix}(R_1)$ (resp. $\mathrm{Fix}(R_2)$), then the

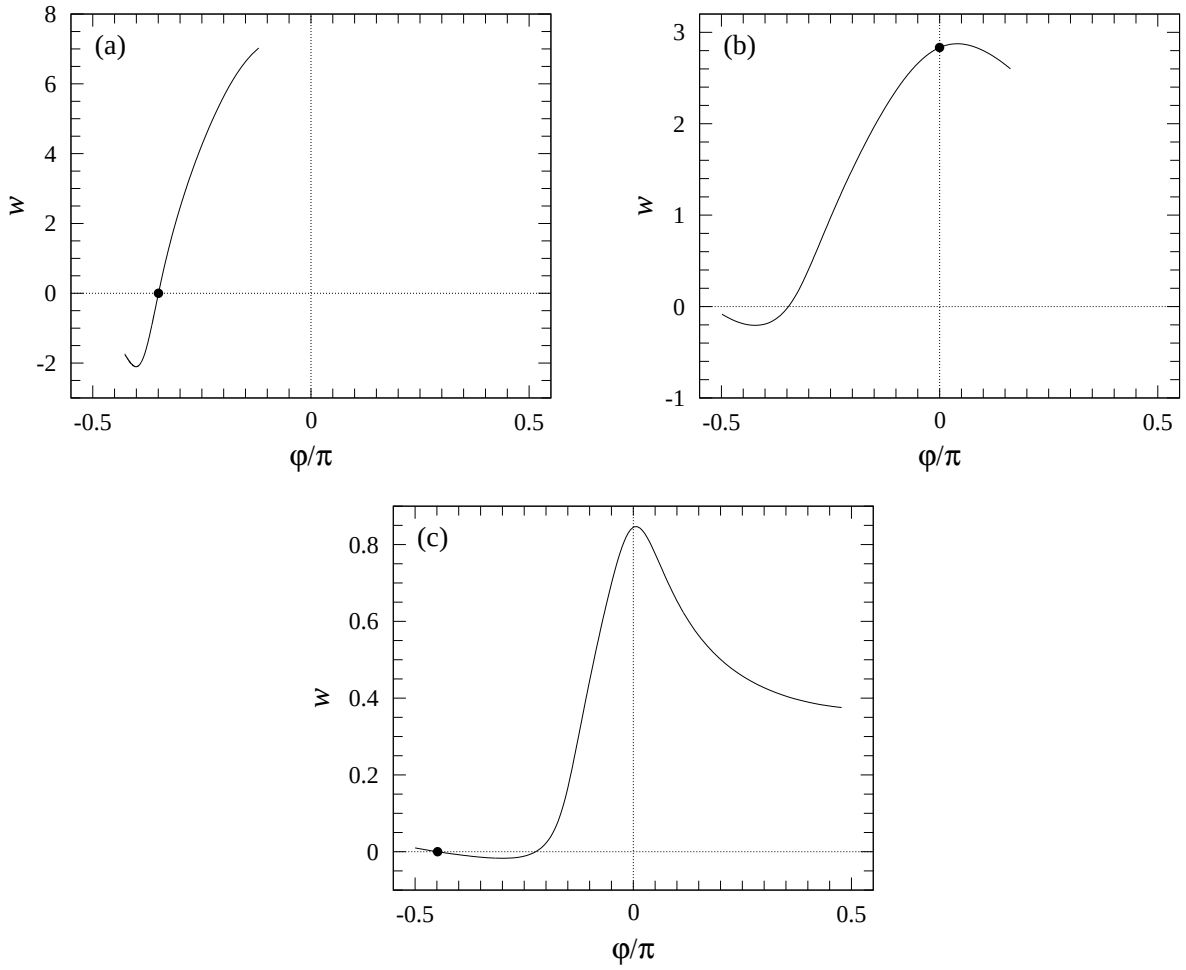

Figure 11. Stable manifold of E_+ on the section Σ: (a) $\alpha = 7$; (b) $\alpha = 1$; (c) $\alpha = 0.1$. The symbol "•"corresponds to heteroclinic orbits which are the limits of one-parameter families of periodic orbits in figures 14, 15 and 16.

intersection gives a heteroclinic orbit from E_+ to E_+^* (resp. to E_-^*).

Similarly, we solve the boundary value problem (2.8) and

$$L_{\rm u}\boldsymbol{\xi}^{\rm s}(0) = \mathbf{0}, \quad \boldsymbol{\xi}^{\rm s}(-T) = \boldsymbol{\xi}_0^{\rm s} \tag{4.3}$$

to compute $W^{\rm s}(E_+)$ numerically, where $L_{\rm u}$ is an 2×4 matrix consisting of row eigenvectors associated with eigenvalues of positive real parts for $\mathrm{D}\boldsymbol{F}(E_+)$, and $\boldsymbol{\xi}_0^{\rm s}$ is a point on $W^{\rm s}(E_+)$. The intersection of $W^{\rm s}(E_+)$ with $\mathrm{Fix}(R_1)$ (resp. $\mathrm{Fix}(R_2)$) gives a heteroclinic orbit from E_+^* (resp. from E_-^*) to E_+. We adopt as a starting solution the analytical heteroclinic orbit (2.21) for $W^{\rm u}(E_+)$ or a small solution of the linearised system (4.1) for $W^{\rm s}(E_+)$, and use the numerical continuation tool AUTO [18] to perform the above computations. In these computations we can also take T and $\boldsymbol{\xi}^{\rm s,u}(0)$ as free parameters.

Figure 9 shows the intersection of $W^{\rm u}(E_+)$ with Σ for $\alpha = 7,\, 1,\, 0.1$. From the figure we see that there are infinitely many heteroclinic orbits from E_+ to E_+^* and E_-^*,

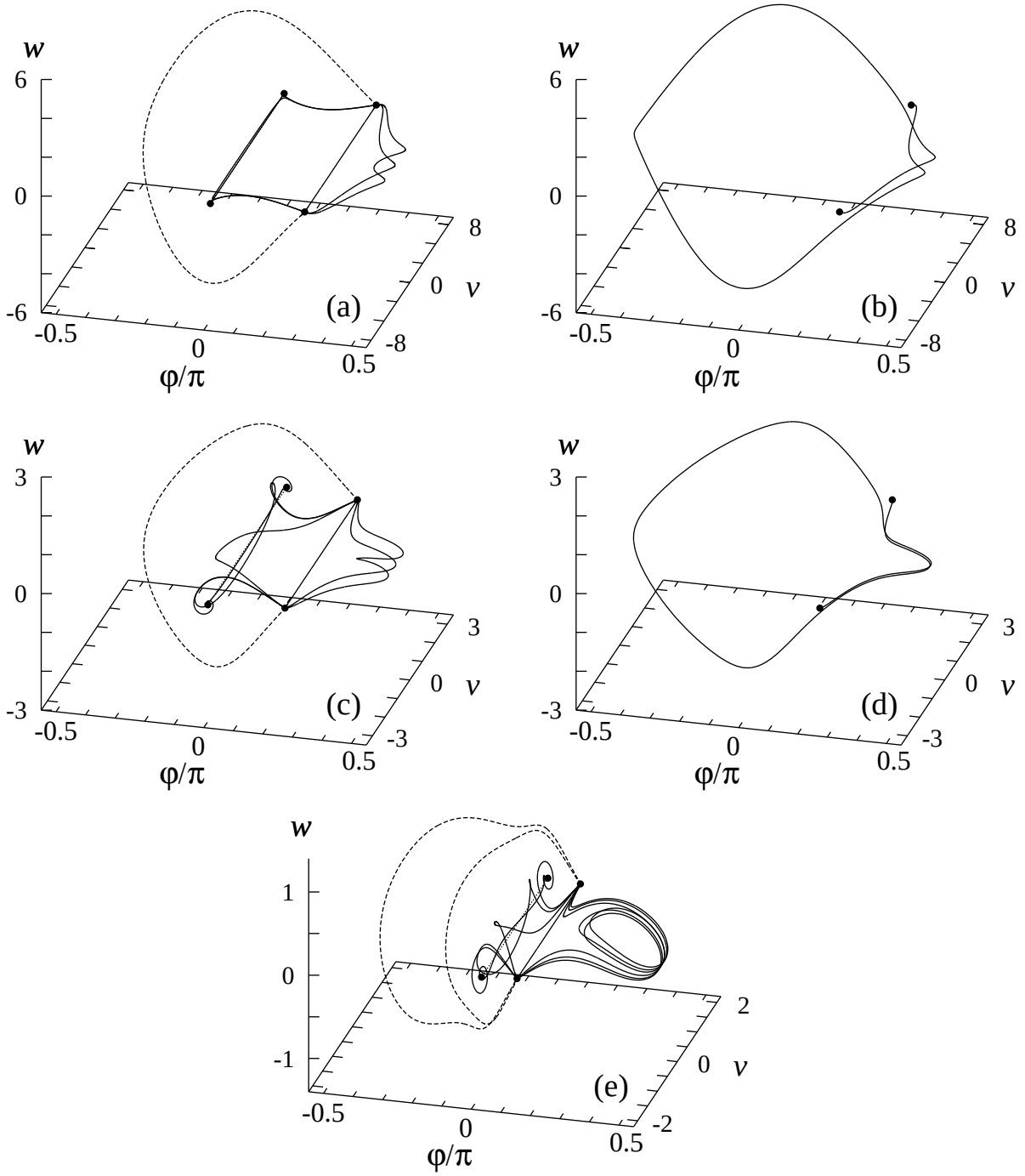

Figure 12. R_1-symmetric heteroclinic connections between E_+ and E_+^*: (a) and (b) $\alpha = 7$; (c) and (d) $\alpha = 1$; (e) $\alpha = 0.1$. Solid (resp. dashed) lines represent heteroclinic orbits from E_+ to E_+^* (resp. from E_+^* to E_+) while dotted lines represent heteroclinic orbits from C to C^*. The symbol "•" represents the equilibrium E_+, E_+^*, C or C^*.

as predicted by theorems 1 and 2. Moreover, $W^{\mathrm{u}}(E_+) \cap \Sigma$ has an isolated, connected component whose right and left ends, respectively, approach a closed curve (the parabolic

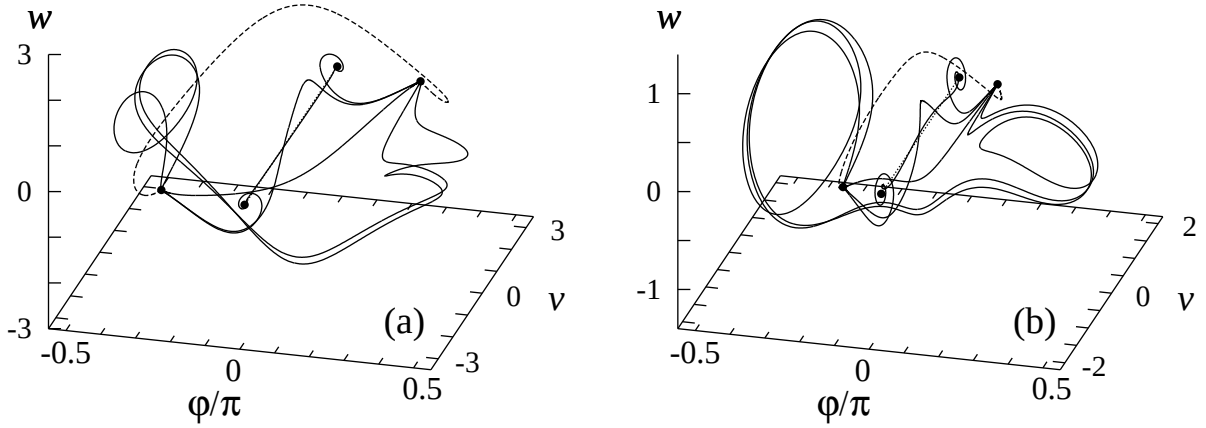

Figure 13. R_2-symmetric heteroclinic connections between E_+ and E_-^*: (a) $\alpha = 1$; (b) $\alpha = 0.1$. Solid (resp. dashed) lines represent heteroclinic orbits from E_+ to E_-^* (resp. from E_-^* to E_+) while dotted lines represent heteroclinic orbits from C to C^*. The symbol "$\bullet$" represents the equilibrium E_+, E_-^*, C or C^*.

manifold $\mathscr{P}_\pm$) and the origin (i.e., a heteroclinic orbit from C to C^*) for $\alpha = 7$, 1, and it has a connected component whose right end lies on $W^{\rm u}(E_+^*) \cap \{r = 0\}$ and whose left end approaches the origin for $\alpha = 0.1$, while it has infinitely many connected components lying between orbits on $W^{\rm u}(E_+^*) \cap \{r = 0\}$, all of which can not be drawn in the figure, in the three cases.

The behaviour of $W^{\rm u}(E_+) \cap \Sigma$ in figure 9(c) for $\alpha = 0.1$ is very different from that in figures 9(a) and (b) for $\alpha = 7$, 1. Figure 10 shows how it changes when the parameter α decreases from $\alpha = 1$. As shown in figure 10(a), a below branch of $W^{\rm u}(E_+) \cap \Sigma$ first approaches the outmost one of the upper-right branches. They touch at $\alpha \approx 0.5884$ and split into right and left after that, as shown in figures 10(b) and (c). When α decreases further, one of the other below branches approaches one of the other upper-right branches (see figure 10(d)), and they touch at $\alpha \approx 0.43201$ and split into right and left (see figures 10(e) and (f)). After similar processes repeatedly occur, $W^{\rm u}(E_+) \cap \Sigma$ finally has such a structure as in figure 9(c) at $\alpha = 0.1$.

Figure 11 shows the intersection of $W^{\rm s}(E_+)$ with the section Σ for $\alpha = 7$, 1, 0.1. Only the part of $\mathscr{E}_0 \le 0$ is depicted there. From the figure we see that there is a heteroclinic orbit from E_-^* to E_+ for $\alpha = 1$, 0.1 as predicted by theorem 3, and that there exists a heteroclinic orbit from E_+^* to E_+ not only for $\alpha = 7$ but also for $\alpha = 1$, 0.1 although theorem 3 says nothing about the latter two cases. In particular, two heteroclinic orbits from E_+^* to E_+ exist for $\alpha = 0.1$. Moreover, our numerical computation indicated $\bar\alpha_1 = 0.37\ldots$, $\alpha_1 = 0$ and $\bar\alpha_2 = \alpha_2 = 2.6\ldots$ in lemma 1 and theorem 3.

Figures 12 and 13, respectively, give R_1- and R_2-symmetric heteroclinic orbits obtained in the computations of figures 11 and 9. We observe heteroclinic orbits from E_+ to E_+^* such that they pass through a heteroclinic orbit from C to C^* (see figures 12(a),(c),(e) and 13) or from E_+^* to E_+ (see figures 12(b) and (d)). Thus, we

numerically found an abundance of heteroclinic connections, as the theory predicted.

4.2. Relative periodic orbits

We now compute periodic orbits predicted by theorem 4 in (2.5), which correspond to relative periodic orbits in the isosceles three-body problem.

We first compute periodic orbits near heteroclinic cycles obtained in section 4.1. We consider the boundary value problem for an eight-dimensional system

$$\dot{\boldsymbol{\xi}}_1 = -\boldsymbol{F}(\boldsymbol{\xi}_1), \quad \dot{\boldsymbol{\xi}}_2 = \boldsymbol{F}(\boldsymbol{\xi}_2) \tag{4.4}$$

under boundary conditions

$$\boldsymbol{\xi}_1(0) = \boldsymbol{\xi}_{10}, \quad \boldsymbol{\xi}_2(0) = \boldsymbol{\xi}_{20}, \quad \boldsymbol{\xi}_1(T_1), \boldsymbol{\xi}_2(T_2) \in \mathrm{Fix}(R_i). \tag{4.5}$$

If $\boldsymbol{\xi}_{10} = \boldsymbol{\xi}_{20}$, then

$$\boldsymbol{\xi}(t) = \begin{cases} \boldsymbol{\xi}_1(-t) & \text{for } t \in [-T_1, 0); \\ \boldsymbol{\xi}_2(t) & \text{for } t \in [0, T_2] \end{cases} \tag{4.6}$$

gives an R_i-symmetric periodic orbit of (2.8) by the reversibility. We solve the boundary value problem and continue the solution with $\boldsymbol{\xi}_{10}$, $\boldsymbol{\xi}_{20}$ or $\Delta\boldsymbol{\xi}_0 = \boldsymbol{\xi}_{10} - \boldsymbol{\xi}_{20}$ till $\Delta\boldsymbol{\xi}_0 = 0$ is satisfied. As the starting solution, we choose a heteroclinic cycle $\{\boldsymbol{\xi}_1(-t), \boldsymbol{\xi}_2(t)\}$ obtained in section 4.1 such that $\boldsymbol{\xi}_1(t) \in W^{\mathrm{s}}(E_+)$ and $\boldsymbol{\xi}_2(t) \in W^{\mathrm{u}}(E_+)$. In this computation we can also take ω, $T_1, T_2 > 0$, $r_j(T_j)$, and $\varphi_j(T_j)$ or $w_j(T_j)$, $j = 1, 2$, as free parameters, where r_j, φ_j and w_j represent components of $\boldsymbol{\xi}_j$.

Next we compute one-parameter families of periodic orbits containing the periodic orbits detected in the above computations. We consider the boundary value problem for (2.8) under boundary conditions

$$\boldsymbol{\xi}(-T_1), \boldsymbol{\xi}(T_2) \in \mathrm{Fix}(R_i). \tag{4.7}$$

By the reversibility, the solution $\boldsymbol{\xi}(t)$ gives an R_i-symmetric periodic orbit of (2.8). We solve the boundary value problem and continue the solution with the angular momentum ω to obtain a one-parameter family of periodic orbits. As the starting solution we take (4.6) for a solution of the boundary value problem (4.4) and (4.5) satisfying $\boldsymbol{\xi}_{10} = \boldsymbol{\xi}_{20}$. In this computation we can also take $T = T_1 + T_2 > 0$, $r(\mp T_j)$, and $\varphi(\mp T_j)$ or $w(\mp T_j)$, $j = 1, 2$, as free parameters. Again, we use the numerical continuation tool AUTO [18] to perform the above computations.

Figures 14, 15 and 16 show numerically computed one-parameter families of R_1- or R_2-symmetric periodic orbits for $\alpha = 7$, 1 and 0.1, respectively. Heteroclinic cycles chosen as starting solutions for each families are indicated in figures 9 and 11. We observe that the one-parameter family contains a both R_1- and R_2-symmetric periodic orbit and lies between a symmetric pair of heteroclinic cycles in figures 14(a)-(c), 15(a)-(c) and 16(b), and that it starts on a heteroclinic cycle and terminates on a periodic orbit with $\omega = 0$ in figures 14(d),(e) and 16(a),(c).

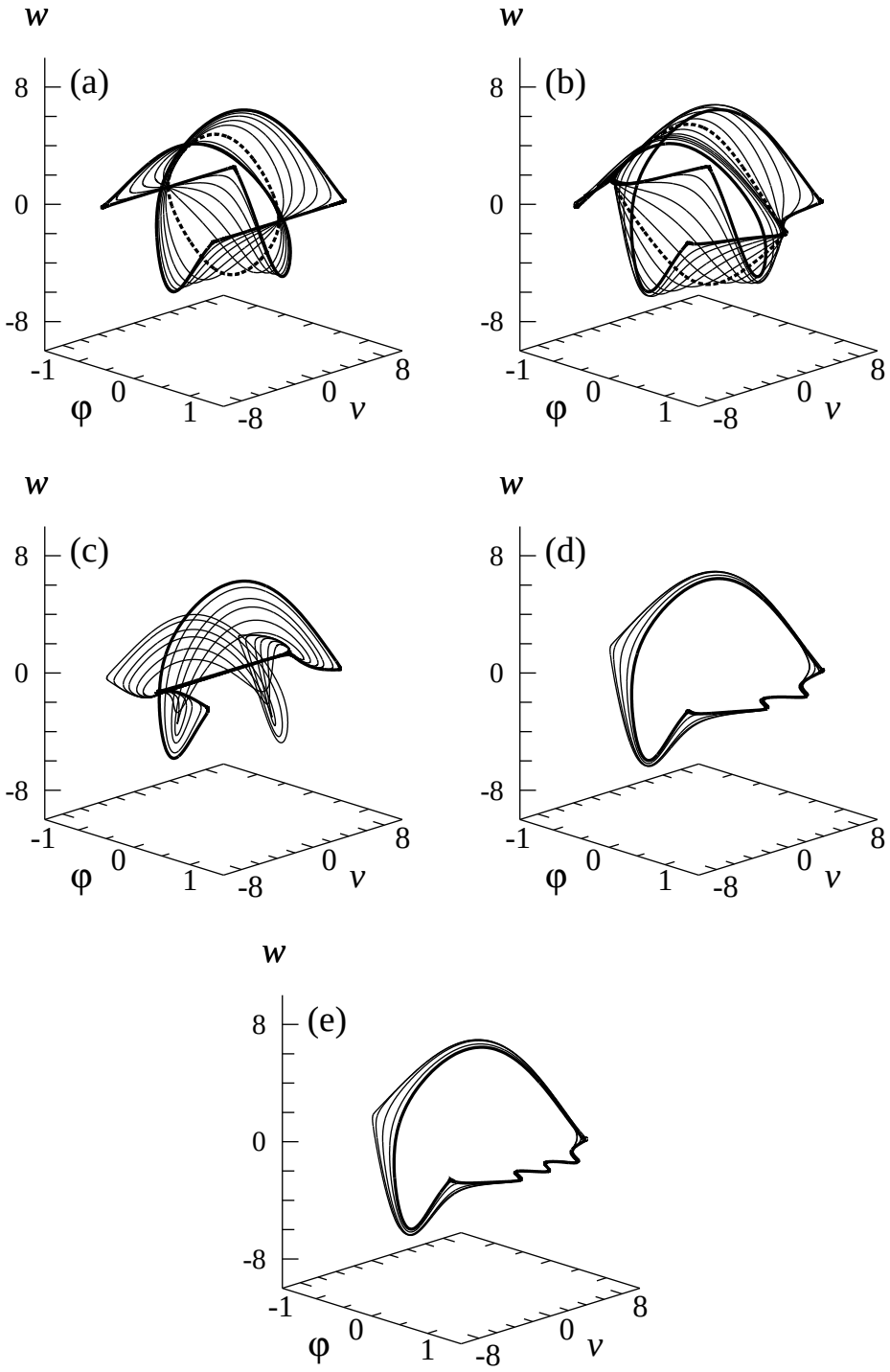

Figure 14. One-parameter families of R_1-symmetric periodic orbits in (2.5) for $\alpha = 7$. Thick solid and dashed lines, respectively, represent periodic orbits near heteroclinic connections and both R_1- and R_2-symmetric periodic orbits.

Finally, we give relative periodic orbits in the isosceles three-body problem which correspond to periodic orbits in figures 14, 15 and 16. We use (2.1)-(2.4) to compute the

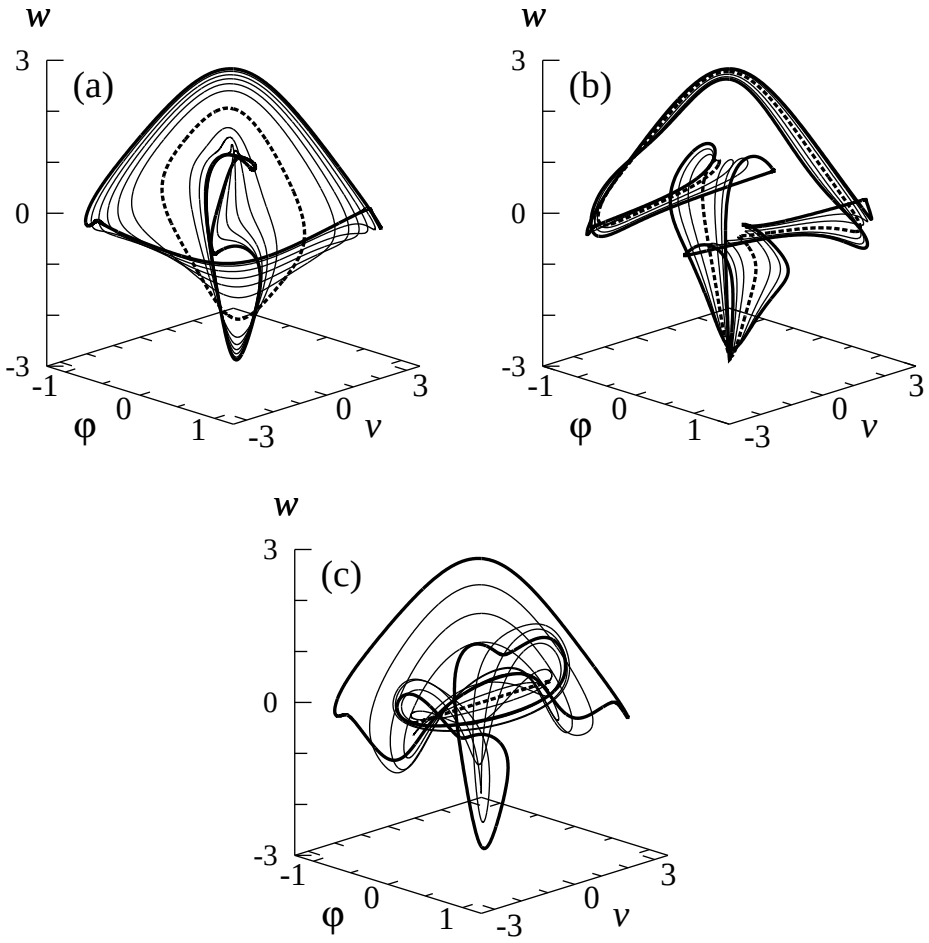

Figure 15. One-parameter families of R_2-symmetric periodic orbits in (2.5) for $\alpha = 1$. Thick solid and dashed lines, respectively, represent periodic orbits near heteroclinic connections and both R_1- and R_2-symmetric periodic orbits.

relative periodic orbits and display them in the rotational $x'y'z$-coordinate system. Note that $x' = r\cos\theta$, $y' = 0$ and $z = \sqrt{\alpha/(\alpha+1)}\, r\sin\theta$.

Figure 17 shows relative periodic orbits corresponding to periodic orbits in figure 14(a) for $\alpha = 7$. The three masses approach very closely and a triple collision almost occurs in figures 17(a) and (e). We easily see that this family consists of symmetric pairs of relative periodic orbits about the x'-axis. Moreover, the relative periodic orbit of figure 17(c) is included in a class theoretically detected by a variational method in [25] and it bifurcates from an Euler orbit. Thus, the obtained relative periodic orbits are closely related to Euler orbits. See [25] for the details. Numerical results revealing this relation are also given there.

Figures 18-21 show relative periodic orbits corresponding to periodic orbits in figure 14(b)-(e) for $\alpha = 7$. Especially, in figure 19(c) the third mass is at rest and the relative periodic orbits is an Euler orbit. Thus, the family of figure 19 bifurcates

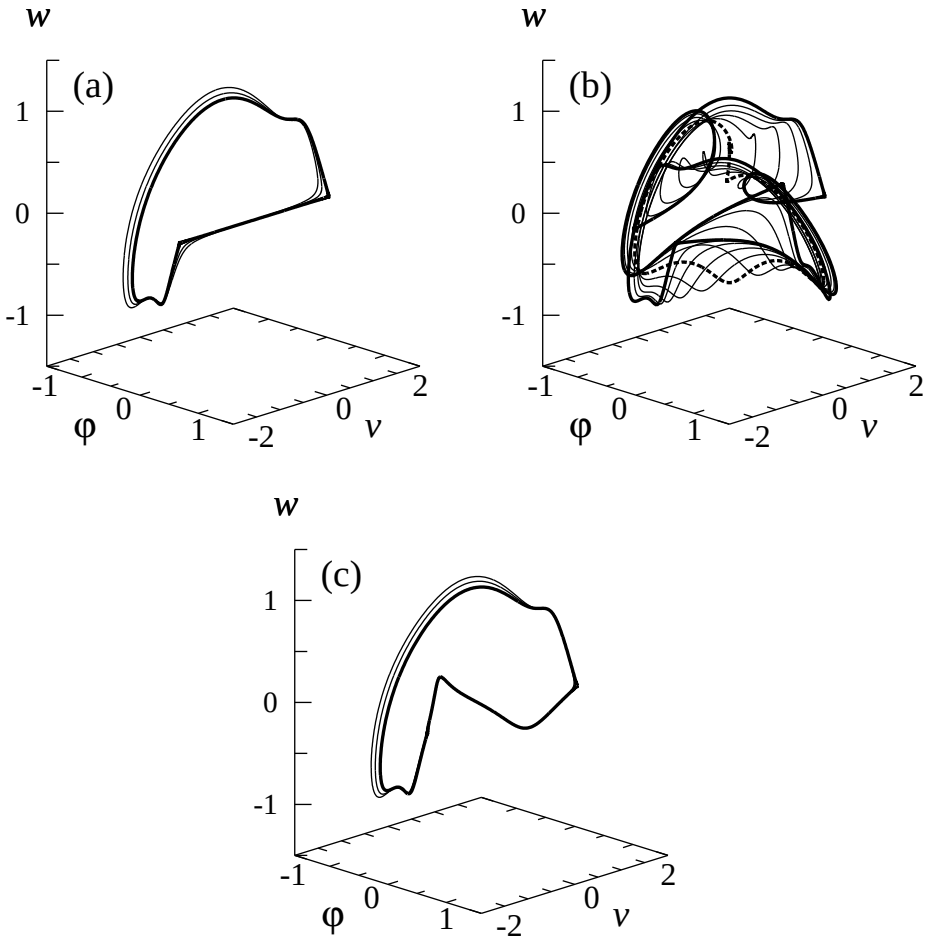

Figure 16. One-parameter families of R_1-symmetric periodic orbits in (2.5) for $\alpha = 0.1$. Thick solid and dashed lines, respectively, represent periodic orbits near heteroclinic connections and both R_1- and R_2-symmetric periodic orbits.

from an Euler orbit. Moreover, we see that one, two and three double collisions almost occur in figures 18(a), 20(a) and 21(a), respectively. This is due to the fact that the corresponding periodic orbits are born from heteroclinic orbits having the same number of double collisions. Again, the relative periodic orbit of figure 18(c) is included in the class theoretically detected in [25] and it bifurcates from an Euler orbit. Although not proven theoretically, it follows from the numerical results of figures 11 and 9 that families of relative periodic orbits similar to those in figures 17-21 also exist for $\alpha = 1,\ 0.1$.

Figures 22-24 and 25-27, respectively, show relative periodic orbits corresponding to periodic orbits in figure 15(a)-(c) for $\alpha = 1$ and in figure 16(a)-(c) for $\alpha = 0.1$. The relative periodic orbits in figure 24(c) is an Euler orbit and the family of figure 19 bifurcates from the Euler orbit. One and two double collisions almost occur in figures 27(a) and 24(a), respectively. In addition, the relative periodic orbits of figure 22(c) and 26(c) are included in the class theoretically detected in [25] and they bifurcate from Euler orbits.

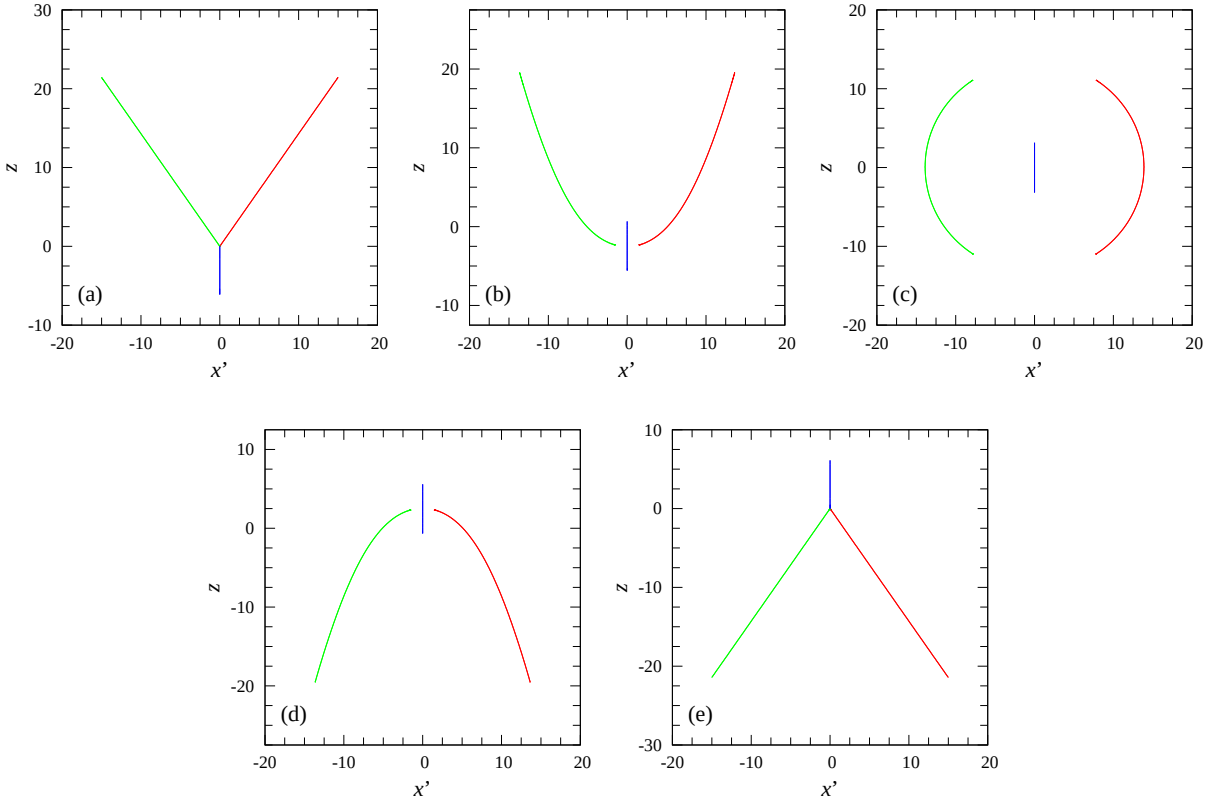

Figure 17. Relative periodic orbits in the isosceles three-body problem for $\alpha = 7$: (a) $\omega = 0.01$; (b) $\omega = 6$; (c) $\omega = 10.6353$; (d) $\omega = 6$; (e) $\omega = 0.01$. These orbits correspond to periodic orbits of figure 14(a).

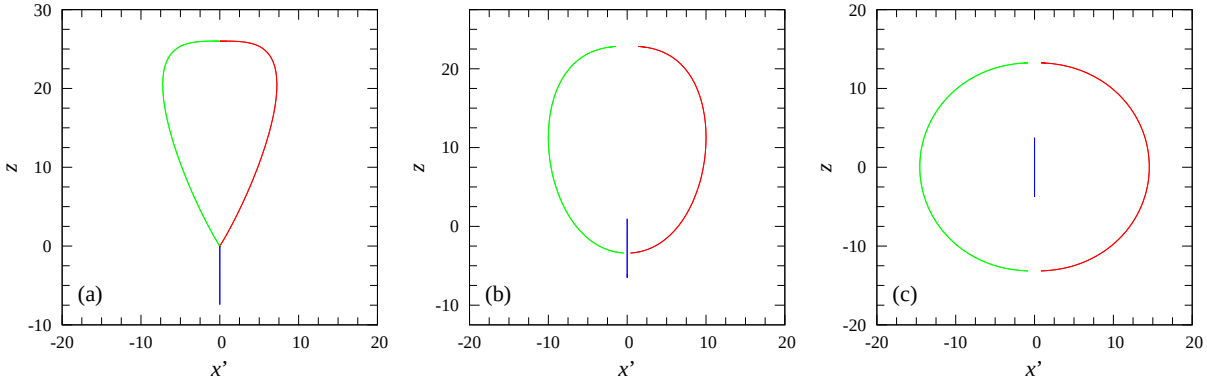

Figure 18. Relative periodic orbits in the isosceles three-body problem for $\alpha = 7$: (a) $\omega = 0.01$; (b) $\omega = 1.69324$; (c) $\omega = 1.61913$. These orbits correspond to periodic orbits of figure 14(b).

Appendix A. Proof of lemma 1

We begin with the proof of part (i). The statement was proved in lemma 1 of [10] for $\alpha \geq \frac{55}{4}$. So we only have to prove it for $\alpha \in [6.52, \frac{55}{4})$. Our proof is also based

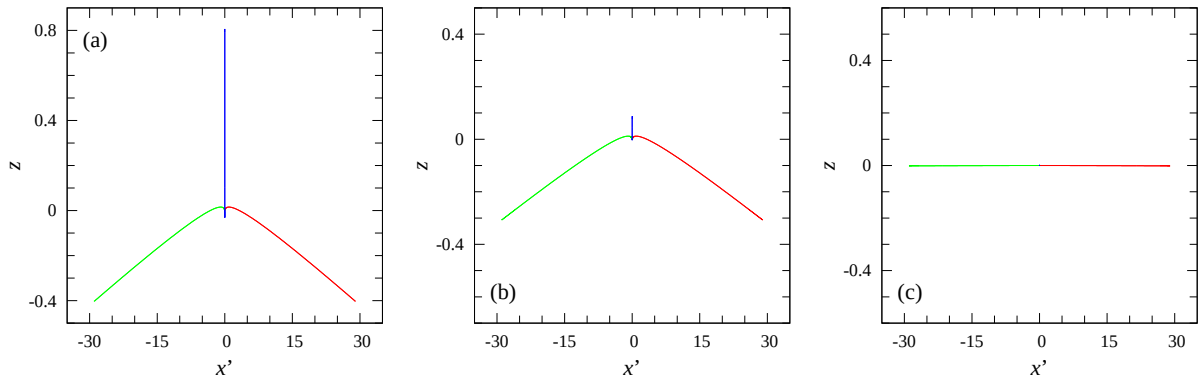

Figure 19. Relative periodic orbits in the isosceles three-body problem for $\alpha = 7$: (a) $\omega = 0.0001$; (b) $\omega = 0.03$; (c) $\omega = 0.0416605$. These orbits correspond to periodic orbits of figure 14(c).

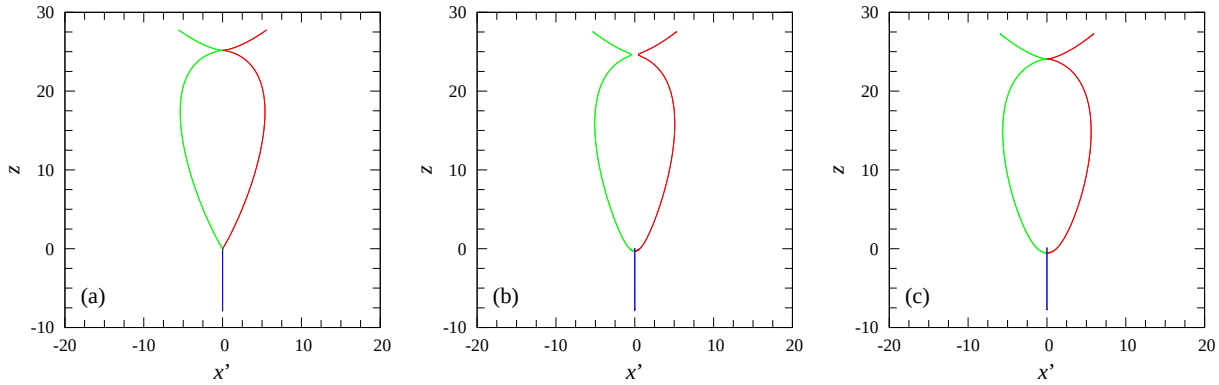

Figure 20. Relative periodic orbits in the isosceles three-body problem for $\alpha = 7$: (a) $\omega = 0.001$; (b) $\omega = 0.918331$; (c) $\omega = 0$. These orbits correspond to periodic orbits of figure 14(d).

on the idea of [10] and assisted by numerical computations: We use a `Matlab` toolbox called `INTLAB` [16], by which we can easily perform self-validating interval arithmetic calculations.

First we rewrite (2.5) on $\mathscr{N}$ as

$$\dot{\varphi} = \pm\sqrt{2U(\varphi) - v^2}, \quad \dot{v} = U(\varphi) - \tfrac{1}{2}v^2$$

in the (φ, v)-coordinates, where the plus and minus signs are taken if w is positive and negative, respectively. Hence, when $v \in (0, v_{\mathrm{c}})$, noting that $\dot{v} > 0$, we can regard φ as a function of v to obtain

$$\frac{\mathrm{d}\varphi}{\mathrm{d}v} = \pm\frac{2}{\sqrt{2U(\varphi) - v^2}}, \tag{A.1}$$

where the sign changes only at $\varphi = \pm\frac{1}{2}\pi$. To detect the loci of $p_+^{\ell,\mathrm{r}}$, we estimate

$$\Delta\varphi = \int_0^{v_{\mathrm{c}}} \frac{2\mathrm{d}v}{\sqrt{2U(\varphi) - v^2}}, \tag{A.2}$$

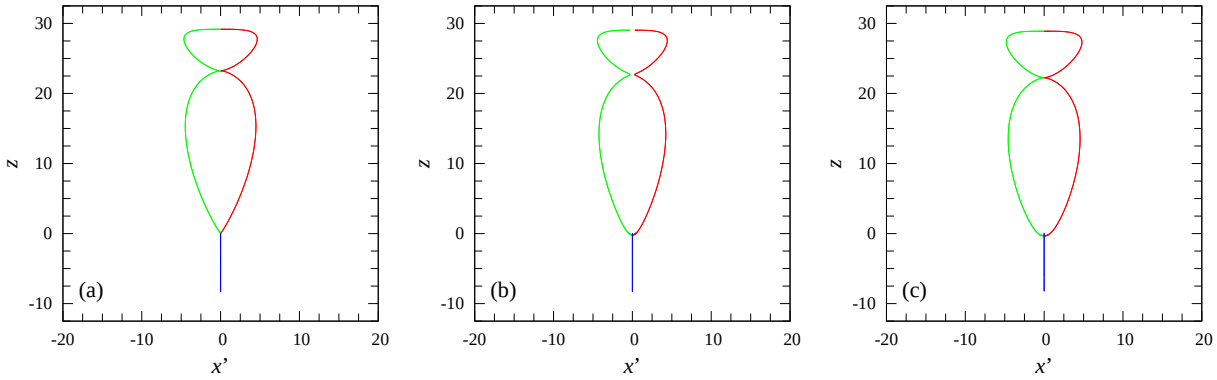

Figure 21. Relative periodic orbits in the isosceles three-body problem for $\alpha = 7$: (a) $\omega = 0.001$; (b) $\omega = 0.753089$; (c) $\omega = 0$. These orbits correspond to periodic orbits of figure 14(e).

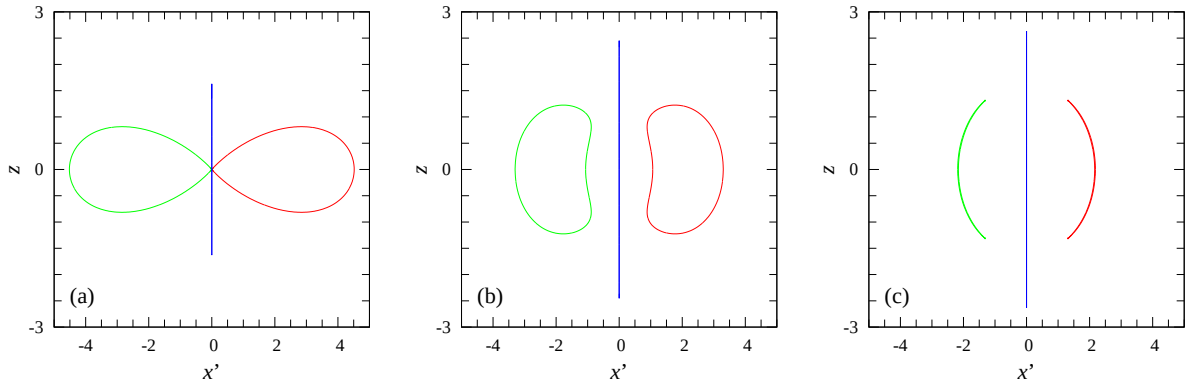

Figure 22. Relative periodic orbits in the isosceles three-body problem for $\alpha = 1$: (a) $\omega = 0.01$; (b) $\omega = 1.5$; (c) $\omega = 1.76706$. These orbits correspond to periodic orbits of figure 15(a).

which represents the total variation of φ while v changes from 0 to v_c, i.e., while an orbit on $W^s(\bar{E}_+)$ moves from Σ to E_+. Letting $\bar{U}(\varphi) = U(\varphi)/U_c$ and changing the variable from v to $\zeta = v/v_c$ in (A.2), we obtain

$$\Delta\varphi = \int_0^1 \frac{2\mathrm{d}\zeta}{\sqrt{\bar{U}(\varphi) - \zeta^2}}. \tag{A.3}$$

Obviously,

$$\Delta\varphi < \int_0^1 \frac{2\mathrm{d}\zeta}{\sqrt{1 - \zeta^2}} = \pi \tag{A.4}$$

since $\bar{U}(\varphi) \geq 1$.

Let $\varphi = \varphi_a > \varphi_c$ be a point at which $\bar{U}(\varphi_a) \geq \bar{U}(0)$. When

$$(\zeta_1, \zeta_2) \in \{\zeta \in [0, 1) \mid |\varphi(\zeta)| \leq \varphi_a\}$$

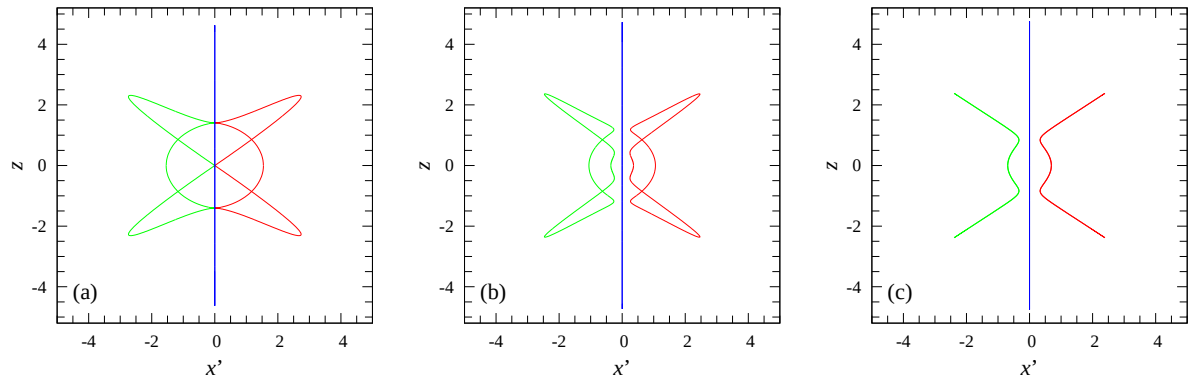

Figure 23. Relative periodic orbits in the isosceles three-body problem for $\alpha = 1$: (a) $\omega = 0.003$; (b) $\omega = 0.7$; (c) $\omega = 0.788677$. These orbits correspond to periodic orbits of figure 15(b).

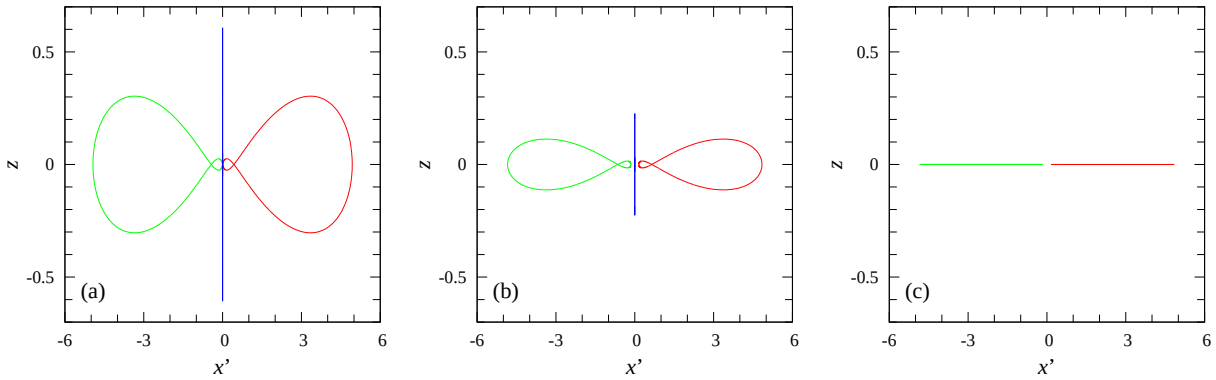

Figure 24. Relative periodic orbits in the isosceles three-body problem for $\alpha = 1$: (a) $\omega = 0.01$; (b) $\omega = 1.2$; (c) $\omega = 1.23862$. These orbits correspond to periodic orbits of figure 15(c).

with $\zeta_1 < \zeta_2$, the variable φ changes by

$$\Delta\varphi_{12} > \int_{\zeta_1}^{\zeta_2} \frac{2\mathrm{d}\zeta}{\sqrt{\zeta_\mathrm{a}^2 - \zeta^2}} = 2\left(\arcsin\left(\frac{\zeta_2}{\zeta_\mathrm{a}}\right) - \arcsin\left(\frac{\zeta_1}{\zeta_\mathrm{a}}\right)\right) \tag{A.5}$$

while ζ changes from ζ_1 to ζ_2, where $\zeta_\mathrm{a} = \sqrt{\bar{U}(\varphi_\mathrm{a})} > 1$. On the other hand, when $|\varphi| > \varphi_\mathrm{a}$, we regard ζ as a function of φ and obtain by (A.1)

$$\begin{aligned}\left|\frac{\mathrm{d}\zeta}{\mathrm{d}\varphi}\right| &\le \tfrac{1}{2}\sqrt{\bar{U}(\varphi)} < \tfrac{1}{2}\sqrt{\frac{1}{U_\mathrm{c}}\left(\sec\varphi + \frac{4\alpha^{3/2}}{\sqrt{\alpha + 2\sin^2\varphi_\mathrm{a}}}\right)} \\ &= \frac{1}{\sqrt{2}\,v_\mathrm{c}}\sqrt{\sec\varphi - \sec\varphi_\mathrm{a} + \tfrac{1}{2}v_\mathrm{c}^2\zeta_\mathrm{a}^2}.\end{aligned}$$

Using a general inequality

$$\sqrt{\mu + \nu} \le \sqrt{\mu} - \sqrt{\mu_0} + \sqrt{\mu_0 + \nu} \quad \text{for } \mu \ge \mu_0 \ge 0 \text{ and } \nu > 0$$

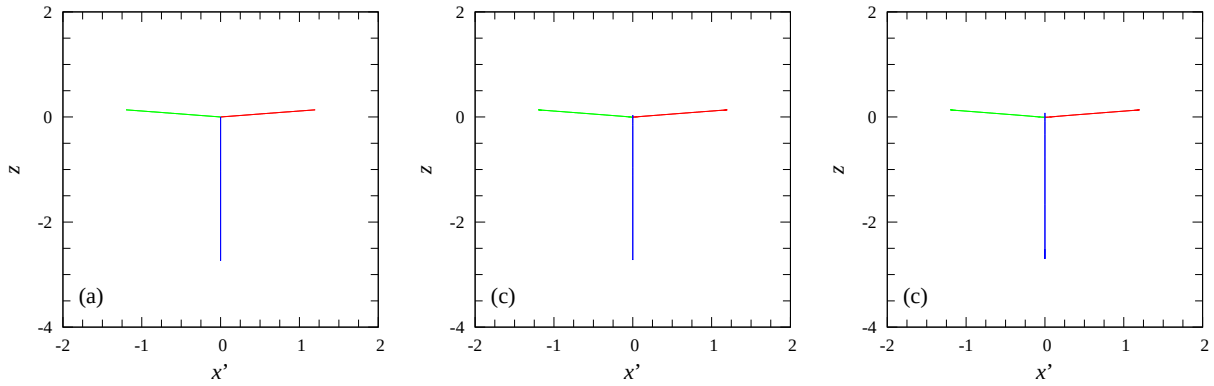

Figure 25. Relative periodic orbits in the isosceles three-body problem for $\alpha = 0.1$: (a) $\omega = 0.001$; (b) $\omega = 0.0314837$; (c) $\omega = 0$. These orbits correspond to periodic orbits of figure 16(a).

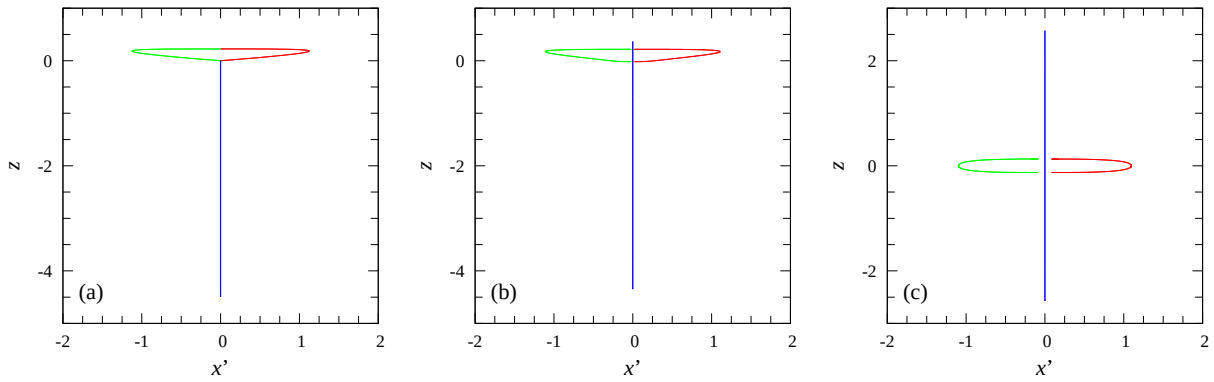

Figure 26. Relative periodic orbits in the isosceles three-body problem for $\alpha = 0.1$: (a) $\omega = 0.001$; (b) $\omega = 0.2$; (c) $\omega = 0.392851$. These orbits correspond to periodic orbits of figure 16(b).

as in the proof of lemma 1 of [10], we get

$$\sqrt{\sec\varphi - \sec\varphi_\mathrm{a} + \tfrac{1}{2}v_\mathrm{c}^2\zeta_\mathrm{a}^2} \le \sqrt{\sec\varphi + 1} - \sqrt{\sec\varphi_\mathrm{a} + 1} + \sqrt{\tfrac{1}{2}}\, v_\mathrm{c}\zeta_\mathrm{a},$$

where we set $\mu = \sec\varphi + 1$, $\mu_0 = \sec\varphi_\mathrm{a} + 1$ and

$$\nu = \tfrac{1}{2}v_\mathrm{c}^2\zeta_\mathrm{a}^2 - \sec\varphi_\mathrm{a} - 1 = U(\varphi_\mathrm{a}) - \sec\varphi_\mathrm{a} - 1 = \frac{4\alpha^{3/2}}{\sqrt{\alpha + 2\sin^2\varphi_\mathrm{a}}} - 1,$$

which is assumed to be positive below (and it is actually positive if $\alpha > 0.541578\ldots$ for any $\varphi_\mathrm{a} \in [0, 2\pi)$). Hence, when φ changes from $\pm\varphi_\mathrm{a}$ to $\pm\frac{1}{2}\pi$ and vice versa, the variable ζ changes by

$$\begin{aligned}\Delta\zeta &< \frac{1}{\sqrt{2}\, v_\mathrm{c}} \int_{\varphi_\mathrm{a}}^{\frac{1}{2}\pi} \left(\sqrt{\sec\varphi + 1} - \sqrt{\sec\varphi_\mathrm{a} + 1} + \sqrt{\tfrac{1}{2}}\, v_\mathrm{c}\zeta_\mathrm{a} \right) \mathrm{d}\varphi \\ &< \frac{1}{\sqrt{2}\, v_\mathrm{c}} \left[(\pi - 2\arctan\sqrt{\sec\varphi_\mathrm{a} - 1}) \right.\end{aligned}$$

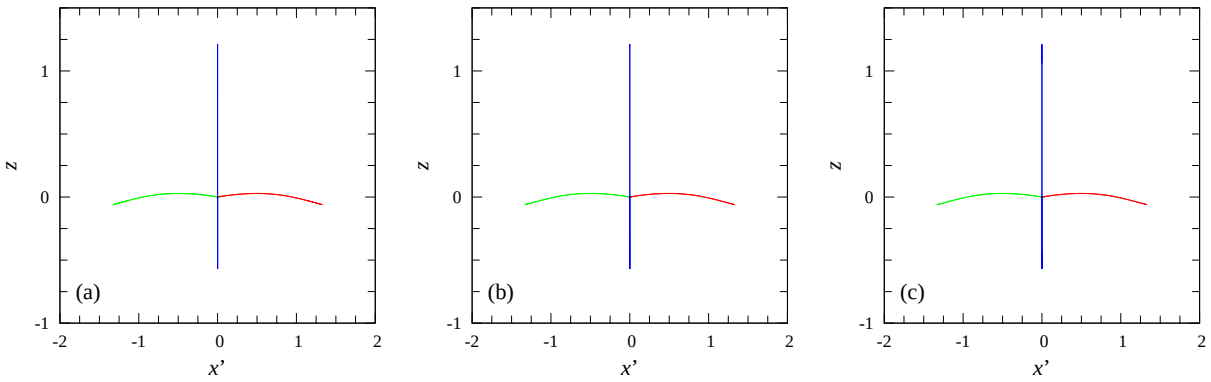

Figure 27. Relative periodic orbits in the isosceles three-body problem for $\alpha = 0.1$: (a) $\omega = 0.001$; (b) $\omega = 0.00691365$; (c) $\omega = 0$. These orbits correspond to periodic orbits of figure 16(c).

$$+\left(\sqrt{\tfrac{1}{2}}\,v_{\rm c}\zeta_{\rm a}-\sqrt{\sec\varphi_{\rm a}+1}\right)\left(\tfrac{1}{2}\pi-\varphi_{\rm a}\right)\Bigg] \tag{A.6}$$

since

$$\frac{d}{{\rm d}\varphi}(2\arctan\sqrt{\sec\varphi-1})=\sqrt{\sec\varphi+1}.$$

Here we note that $U_{\rm c}$ and $v_{\rm c}$ are increasing functions of α and

$$\bar{U}(0)=\frac{(4\alpha+1)\sqrt{\alpha+2}}{\sqrt{2(2\alpha+1)^3}}$$

is an increasing and decreasing function of α in $[0,\frac{5}{8})$ and in $(\frac{5}{8},\infty)$, respectively. Moreover, we show that $\bar{U}(\varphi)$ is a decreasing function of α for φ fixed in any α-interval satisfying $\varphi>\varphi_{\rm c}$ as follows. First, we easily see that

$$\frac{\partial}{\partial\alpha}(U(\varphi)-U_{\rm c})<0. \tag{A.7}$$

Choose any α_* and φ_* and let $\kappa_*=\bar{U}(\varphi_*)$ with $\alpha=\alpha_*$. Then $U(\varphi_*)-\kappa_*U_{\rm c}<0$ at $\alpha>\alpha_*$ since $\kappa_*>1$ and

$$\frac{\partial}{\partial\alpha}(U(\varphi)-\kappa_*U_{\rm c})<0$$

by (A.7). Hence, $\bar{U}(\varphi_*)<\kappa_*$ for $\alpha>\alpha_*$, which verifies our claim.

Now, in an α-interval $[\tilde{\alpha}_1,\tilde{\alpha}_2)$ given, we can show that $\Delta\varphi>\frac{1}{2}\pi+\varphi_{\rm c}$ (recall that $\Delta\varphi$ is given in (A.2) or (A.3)) for an orbit arriving at p_+^ℓ as follows. Suppose in contradiction to the claim that $\Delta\varphi\le\frac{1}{2}\pi+\varphi_{\rm c}$. Then, we have $|\varphi(\zeta)|\le\varphi_{\rm a}$ for $\zeta\in(\Delta\zeta,1)$ and use (A.5) with $\zeta_1=\Delta\zeta$ and $\zeta_2=1$ to obtain

$$\varphi_{\rm a}+\varphi_{\rm c}>2\left(\arcsin\left(\frac{1}{\zeta_{\rm a}}\right)-\arcsin\left(\frac{\Delta\zeta}{\zeta_{\rm a}}\right)\right). \tag{A.8}$$

We take $\varphi_{\rm a}$ for each $\alpha\in[\tilde{\alpha}_1,\tilde{\alpha}_2)$ such that $\zeta_{\rm a}$ is the same and greater than but close to $\sqrt{\bar{U}(0)}$ with $\alpha=\tilde{\alpha}_1$, and choose $\varphi_{{\rm a},j}$, $j=1,2$, such that $\varphi_{{\rm a},j}$ is close to $\varphi_{\rm a}$ at $\alpha=\tilde{\alpha}_j$

Table A1. Self-validating computations via the `Matlab` toolbox `INTLAB` for the proof of part (i) of lemma 1. Here the u.b. of $\Delta\zeta$ and the l.b. of $\psi_{\rm c}$ are estimated by (A.6) and (A.8), respectively, where "u.b." and "l.b." denote upper and lower bounds, respectively.

$[\tilde{\alpha}_1, \tilde{\alpha}_2)$	$\zeta_{\rm a}$	$\varphi_{\rm a,1}$	$\varphi_{\rm a,2}$	u.b. of $\Delta\zeta$	l.b. of $\varphi_{\rm c}$	$\varphi_{\rm c}(\tilde{\alpha}_2)$
$[9.1, \frac{55}{4})$	1.02338	1.33492	1.38010	0.159783	1.01961	1.0173...
$[7.6, 9.1)$	1.02717	1.32980	1.35057	0.167015	1.00335	1.0031...
$[7.1, 7.6)$	1.02872	1.32763	1.33568	0.170017	1.00015	0.9952...
$[6.8, 7.1)$	1.02973	1.32616	1.33132	0.172016	0.992839	0.9918...
$[6.65, 6.8)$	1.03027	1.32541	1.32810	0.173056	0.989939	0.9896...
$[6.58, 6.65)$	1.03053	1.32505	1.32634	0.173555	0.988772	0.9884...
$[6.55, 6.58)$	1.03064	1.32489	1.32545	0.173774	0.988410	0.9879...
$[6.53, 6.55)$	1.03071	1.324768	1.325138	0.1739283	0.98789	0.9876...
$[6.52, 6.53)$	1.03075	1.32472	1.32491	0.173999	0.98768	0.9875...

but $\varphi_{\rm a,1} < \varphi_{\rm a}$ at $\alpha = \tilde{\alpha}_1$ and $\varphi_{\rm a,2} > \varphi_{\rm a}$ at $\alpha = \tilde{\alpha}_2$. Then we have $\varphi_{{\rm a},j} < \varphi_{\rm a} < \varphi_{\rm a,2}$ for $\alpha \in [\tilde{\alpha}_1, \tilde{\alpha}_2)$ since $\bar{U}(\varphi)$ is a decreasing function of α for φ fixed and an increasing function of φ for α fixed when $\varphi > \varphi_{\rm c}$. Thus, the upper bound of $\Delta\zeta$ is estimated by (A.6) with $\alpha = \alpha_1$ and $\varphi_{\rm a} = \varphi_{\rm a,1}$. Finally, we use (A.8) with $\varphi_{\rm a} = \varphi_{\rm a,2}$ and estimate the lower bound of $\varphi_{\rm c}$, which may yield a contradiction: it may be greater than $\varphi_{\rm c}$ for $\alpha = \tilde{\alpha}_2$. This means that $\Delta\varphi > \frac{1}{2}\pi + \varphi_{\rm c}$ in $[\tilde{\alpha}_1, \tilde{\alpha}_2)$ as in the claim.

We divide the α-interval $[6.52, \frac{55}{4})$ into nine subintervals and numerically carry out the above procedure in a self-validating way via the `Matlab` toolbox `INTLAB` to show that $\Delta\varphi > \frac{1}{2}\pi + \varphi_{\rm c}$ in the α-interval. The numerical computation results are summarised in table A1. Thus, we prove along with (A.4) that $p_+^\ell \in \{\varphi < 0, w < 0\}$ in the α-interval. Note that the value of $\bar{\alpha}_1 = 6.52$ is not optimal and our computation can still be extended to a slightly lower value.

Next assume that $\Delta\varphi \le \frac{1}{2}\pi - \varphi_{\rm c}$ for an orbit arriving at $p_+^{\rm r}$ and let the orbit pass through $\varphi = \varphi_{\rm a}$ at $\zeta = \zeta_1$. Since $\varphi < \varphi_{\rm a}$ for $\zeta > \zeta_1$, as in (A.5), the variable φ changes by

$$\Delta\varphi_1 > \int_{\zeta_1}^{1} \frac{2{\rm d}\zeta}{\sqrt{\zeta_{\rm a}^2 - \zeta^2}} = 2\left(\arcsin\left(\frac{1}{\zeta_{\rm a}}\right) - \arcsin\left(\frac{\zeta_1}{\zeta_{\rm a}}\right)\right) \tag{A.9}$$

when ζ changes from $\zeta = \zeta_1$ to 1. Moreover, the upper bound of the change of ζ when φ increases from $\varphi_{\rm a}$ to $\Delta\varphi + \varphi_{\rm c}$ is given by the right hand side of (A.6). From table A1 we have $\zeta_{\rm a} < 1.0375$ and $\zeta_1 < 0.173999$ for $\alpha \in [6.52, \frac{55}{4}]$. So we estimate (A.9) as

$$\Delta\varphi_1 > 2\left(\arcsin\left(\frac{1}{1.0375}\right) - \arcsin\left(\frac{0.173999}{1.0375}\right)\right) > 2.265 > \frac{\pi}{2},$$

which yields a contradiction. Hence, we have $\Delta\varphi > \frac{1}{2}\pi - \varphi_{\rm c}$ which means $p_+^{\rm r} \in \{w > 0\}$. Thus, we complete the proof of part (i).

We turn to the proof of part (ii). First, we easily see that $\Delta\varphi > \varphi_{\rm c}$ for an orbit arriving at p_+^ℓ, as follows. Assume that this is not true, i.e., $\Delta\varphi \le \varphi_{\rm c}$ for the orbit. Then

$\bar{U}(\varphi) < \bar{U}(0)$ so that by (A.3)

$$\Delta\varphi > \int_0^1 \frac{2\mathrm{d}\zeta}{\sqrt{\zeta_0^2 - \zeta^2}} = 2\arcsin\left(\frac{1}{\zeta_0}\right) > \tfrac{1}{2}\pi > \varphi_\mathrm{c}, \quad \zeta_0 = \sqrt{\bar{U}(0)},$$

which yields a contradiction, since $\sqrt{\bar{U}(0)} \le \sqrt[4]{\frac{7^3}{3^5}} = 1.0899\ldots$. Hence we have $\Delta\varphi > \varphi_\mathrm{c}$, so that $p_+^\ell \in \{\varphi < 0\}$.

We can also show that $\Delta\varphi < \pi - \varphi_\mathrm{c}$ for an orbit arriving at p_+^r in an α-interval $[\tilde{\alpha}_1, \tilde{\alpha}_2)$ given, as follows. Suppose the contradiction that $\Delta\varphi \ge \pi - \varphi_\mathrm{c}$ and let the orbit pass through $\varphi = \varphi_\mathrm{a}$ at $\zeta = \zeta_3, \zeta_4$ $(0 < \zeta_3 < \zeta_4 < 1)$. Recall that $\varphi_\mathrm{a} (> \varphi_\mathrm{c})$ satisfies $\bar{U}(\varphi_\mathrm{a}) \ge \bar{U}(0)$. As in (A.6), the variable φ changes by

$$\pi - \varphi_\mathrm{a} < \int_0^{\zeta_3} \frac{2 \ \ d\zeta}{\sqrt{1-\zeta^2}} = 2\arcsin\zeta_3 \tag{A.10}$$

and

$$\varphi_\mathrm{a} - \varphi_\mathrm{c} < \int_{\zeta_4}^1 \frac{2 \ \ d\zeta}{\sqrt{1-\zeta^2}} = \pi - 2\arcsin\zeta_4 \tag{A.11}$$

while ζ changes from $\zeta = 0$ to ζ_3, and from ζ_4 to 1, respectively, since $\bar{U}(\varphi) \ge 1$. Combining (A.10) and (A.11), we obtain

$$\zeta_4 - \zeta_3 < \cos\tfrac{1}{2}(\varphi_\mathrm{a} - \varphi_\mathrm{c}) - \cos\tfrac{1}{2}\varphi_\mathrm{a}. \tag{A.12}$$

On the other hand, when $\zeta_3 \le \zeta \le \zeta_4$ so that $\varphi \ge \varphi_\mathrm{a}$, we have via (A.1)

$$\begin{aligned}\left|\frac{\mathrm{d}\zeta}{\mathrm{d}\varphi}\right| &> \tfrac{1}{2}\sqrt{\bar{U}(\varphi) - 1} \ge \tfrac{1}{2}\sqrt{\frac{1}{U_\mathrm{c}}\left(\sec\varphi + \frac{4\alpha^{3/2}}{\sqrt{\alpha + 2\sin^2\varphi_\mathrm{a}}} - U_\mathrm{c}\right)} \\ &> \frac{1}{\sqrt{2}\,v_\mathrm{c}}\sqrt{\sec\varphi - \sec\varphi_\mathrm{a}} > \frac{1}{\sqrt{2}\,v_\mathrm{c}}\left(\sqrt{\sec\varphi + 1} - \sqrt{\sec\varphi_\mathrm{a} + 1}\right).\end{aligned}$$

Hence,

$$\begin{aligned}\zeta_4 - \zeta_3 &> \frac{\sqrt{2}}{v_\mathrm{c}}\int_{\varphi_\mathrm{a}}^{\frac{1}{2}\pi}\left(\sqrt{\sec\varphi + 1} - \sqrt{\sec\varphi_\mathrm{a} + 1}\right)\mathrm{d}\varphi \\ &> \frac{\sqrt{2}}{v_\mathrm{c}}\left[(\pi - 2\arctan\sqrt{\sec\varphi_\mathrm{a} - 1}) - \left(\tfrac{1}{2}\pi - \varphi_\mathrm{a}\right)\sqrt{\sec\varphi_\mathrm{a} + 1}\right].\end{aligned} \tag{A.13}$$

Noting that $\bar{U}(0)$ is an increasing (resp. decreasing) function of α in $[0, \frac{5}{8})$ (resp. in $[\frac{5}{8}, \infty)$), we take φ_a for each $\alpha \in (\tilde{\alpha}_1, \tilde{\alpha}_2]$ with $\tilde{\alpha}_2 \le \frac{5}{8}$ (resp. $\tilde{\alpha}_1 \ge \frac{5}{8}$) such that ζ_a is the same and greater than but close to $\sqrt{\bar{U}(0)}$ with $\alpha = \tilde{\alpha}_2 < \frac{5}{8}$ (resp. with $\alpha = \tilde{\alpha}_1$), and choose $\varphi_{\mathrm{a},j}$, $j = 1, 2$, such that $\varphi_{\mathrm{a},j}$ is close to φ_a at $\alpha = \tilde{\alpha}_j$ but $\varphi_{\mathrm{a},1} < \varphi_\mathrm{a}$ at $\alpha = \tilde{\alpha}_1$ and $\varphi_{\mathrm{a},2} > \varphi_\mathrm{a}$ at $\alpha = \tilde{\alpha}_2$. We easily see that $\varphi_{\mathrm{a},1} < \varphi_\mathrm{a} < \varphi_{\mathrm{a},2}$ for $\alpha \in (\tilde{\alpha}_1, \tilde{\alpha}_2]$, as before. Hence, the upper bound of $\zeta_4 - \zeta_3$ can estimated by (A.12) with $\varphi_\mathrm{a} = \varphi_{\mathrm{a},2}$ and φ_c at $\alpha = \tilde{\alpha}_2$ and its lower bound can be estimated by (A.13) with $\varphi_\mathrm{a} = \varphi_{\mathrm{a},2}$ and v_c at $\alpha = \tilde{\alpha}_2$, since φ_c and v_c are increasing functions of α. These estimates may yield a contradiction, which means that $\Delta\varphi < \pi - \varphi_\mathrm{c}$ in $(\tilde{\alpha}_1, \tilde{\alpha}_2]$ as in the claim.

Table A2. Self-validating computations via the `Matlab` toolbox `INTLAB` for the proof of part (ii) of lemma 1. Here the u.b. and l.b. of $\zeta_4 - \zeta_3$ are estimated by (A.12) and (A.13), respectively.

$(\tilde{\alpha}_1, \tilde{\alpha}_2]$	$\zeta_{\rm a}$	$\varphi_{\rm a,2}$	u.b. of $\zeta_4 - \zeta_3$	l.b. of $\zeta_4 - \zeta_3$
$(0, \frac{5}{8}]$	1.08999	1.09122	0.126281	0.372895
$(\frac{5}{8}, 1.9]$	1.08999	1.28358	0.178655	0.186277
$(1.9, 2.1]$	1.06863	1.26363	0.175827	0.183098
$(2.1, 2.23]$	1.06537	1.26661	0.177081	0.177123
$(2.23, 2.25]$	1.06339	1.26410	0.176660	0.177017

We divide the α-interval $(\frac{5}{8}, 2.25]$ into four subintervals and numerically carry out the above procedure for five subintervals including $(0, \frac{5}{8}]$ in a self-validating way via the `Matlab` toolbox `INTLAB` to show that $\Delta\varphi < \pi - \varphi_{\rm c}$ in the α-interval $(0, 2.25]$. The numerical computation results are summarised in table A2. Thus, we prove that $p^{\rm r}_{+} \in \{\varphi > 0, w > 0\}$ in the α-interval. This completes the proof of part (ii). □

Acknowledgments

M.S. was partially supported by the Global COE Program "Fostering Top Leaders in Mathematics — Broadening the Core and Exploring New Ground" from the Ministry of Education, Culture, Sports, Science and Technology of Japan, and by the Japan Society for the Promotion of Science (JSPS) and Russian Foundation for Basic Research under the Japan-Russia Research Cooperative Program. K.Y. was partially supported by the JSPS, Grant-in-Aid for Scientific Research (C) #18560056. The authors thank Shinya Miyajima at Gifu University for his advice in the use of the `Matlab` toolbox `INTLAB`.

References

[1] Meyer K R, Hall G R and Offin D 2009 *Introduction to Hamiltonian Dynamical Systems and the N-body Problem* 2nd ed (New York: Springer)

[2] Chenciner A and Montgomery R 2000 A remarkable periodic solution of the three-body problem in the case of equal masses *Ann. Math.* **152** 881–901

[3] Chenciner A, Féjoz J and Montgomery R 2005 Rotating Eights: I. The three Γ_i families *Nonlinearity* **18** 1407–1424

[4] Marchal C 2000 The family P12 of the three-body problem: The simplest family of periodic orbits with twelve symmetries per period *Cel. Mech. Dynam. Astron.* **78** 279–98

[5] Chenciner A and Féjoz J 2009 Unchained polygons and the N-body problem *Regul. Chaotic Dyn.* **14** 64–115

[6] McGehee R 1974 Triple collision in the collinear three-body problem *Invent. Math.* **27** 191–227

[7] Devaney R L 1980 Triple collision in the planar isosceles three-body problem *Invent. Math.* **60** 249–267

[8] Devaney R L 1981 Singularities in classical mechanical systems *Ergodic theory and dynamical systems I* ed A. Katok (Boston: Birkhäuser) 211–333

[9] Simó C 1980 Analysis of triple collision in the isosceles problem *Classical Mechanics and Dynamical System* ed R L Devaney and Z H Nitecki (New York: Marcel Dekker) 203–224
[10] Moeckel R 1981 Orbits of the three-body problem which pass infinitely close to triple collision *Amer. J. Math.* **103** 1323–1341
[11] Moeckel R 1984 Heteroclinic phenomena in the isosceles three-body problem *SIAM J. Math. Anal.* **15** 857–876
[12] Simó C and Martínez R 1987/88 Qualitative study of the planar isosceles three-body problem *Celestial Mech.* **41** 179–251
[13] Shibayama M Free-fall orbits and heteroclinic orbits to triple collisions, and shadowing in the isosceles three-body problem, submitted (the preprint is available at `http://www.kurims.kyoto-u.ac.jp/preprint/preprint_y2009.html`)
[14] Easton R W 1975 Isolating blocks and symbolic dynamcis *J. Diff. Eqns* **17** 96–118
[15] Moeckel R 2007 Symbolic dynamics in the planar three-body problem *Regul. Chaotic Dyn.* **12** 449–475
[16] Rump S M 1999 INTLAB - INTerval LABoratory *Developments in Reliable Computing* ed T. Csendes (Dordrecht: Kluwer) 77–104 (available at `http://www.ti3.tu-harburg.de/rump/`).
[17] Devaney R L 1977 Blue sky catastrophes in reversible and Hamiltonian systems *Ind. Univ. Math. J.* **26** 247–263
[18] Doedel E, Champneys A R, Fairgrieve T F, Kuznetsov, Y A, Sandstede B and Wang X 1997 *AUTO97: Continuation and Bifurcation Software for Ordinary Differential Equations (with HomCont)* Concordia University, Montreal (available at `http://cmvl.cs.concordia.ca/auto/`).
[19] Lamb J S W and Roberts J A G 1998 Time-reversal symmetry in dynamical systems: a survey *Physica D* **112** 1–39
[20] Vanderbauwhede A and Fiedler B 1992 Homoclinic period blow-up in reversible and conservative systems *Z. Angew. Math. Phys.* **43** 292–318
[21] McGehee R 1973 A stable manifold theorem for degenerate fixed points with applications to celestial mechanics *J. Differential Equations* **14** 70–88
[22] Andronov A A, Leontovich E A, Gordon I I and Maier A G 1971 *Theory of Bifurcations of Dynamical Systems on a Plane* (Jerusalem: Israel Program of Scientific Translations)
[23] Doedel E J, Krauskopf B and Osinga H M 2006 Global bifurcations of the Lorenz manifold *Nonlinearity* **19** 2947-2972
[24] Yagasaki K Numerical computation of stable and unstable manifolds of normally hyperbolic invariant manifolds, in preparation
[25] Shibayama M and Yagasaki K KAM stability and bifurcations of the Euler solutions in the isosceles three-body problem, in preparation